Applied Research Laboratory

Technical Report

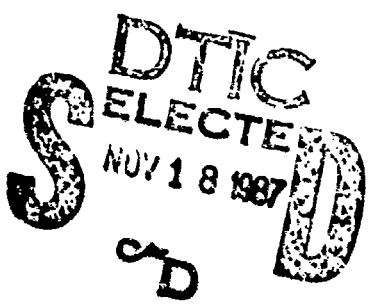

PENNSTATE

(12)

The Pennsylvania State University
APPLIED RESEARCH LABORATORY
P.O. Box 30
State College, PA 16804

A FRACTAL ANALYSIS OF BRITTLE FRACTURE

by

T. J. Mackin and J. J. Mecholsky

Technical Report No. TR 87-007
October 1987

Supported by:
Naval Sea Systems Command

L. R. Hettche
Applied Research Laboratory

Unclassified
SECURITY CLASSIFICATION OF THIS PAGE

A188334

REPORT DOCUMENTATION PAGE

1a. REPORT SECURITY CLASSIFICATION Unclassified	1b. RESTRICTIVE MARKINGS
2a. SECURITY CLASSIFICATION AUTHORITY	3. DISTRIBUTION / AVAILABILITY OF REPORT (A) Unlimited
2b. DECLASSIFICATION / DOWNGRADING SCHEDULE	
4. PERFORMING ORGANIZATION REPORT NUMBER(S) TR-87-007	5. MONITORING ORGANIZATION REPORT NUMBER(S)
6a. NAME OF PERFORMING ORGANIZATION Applied Research Laboratory The Penna. State University 6b. OFFICE SYMBOL (If applicable) ARL	7a. NAME OF MONITORING ORGANIZATION Naval Sea Systems Command Department of the Navy
6c. ADDRESS (City, State, and ZIP Code) P. O. Box 30 State College, PA 16804	7b. ADDRESS (City, State, and ZIP Code) Washington, DC 20362
8a. NAME OF FUNDING / SPONSORING ORGANIZATION Naval Sea Systems Command 8b. OFFICE SYMBOL (If applicable) NAVSEA	9. PROCUREMENT INSTRUMENT IDENTIFICATION NUMBER N-00024-85-C-6041
8c. ADDRESS (City, State, and ZIP Code) Department of the Navy Washington, DC 20362	10. SOURCE OF FUNDING NUMBERS PROGRAM ELEMENT NO. / PROJECT NO. / TASK NO. / WORK UNIT ACCESSION NO

11. TITLE (Include Security Classification)
A FRACTAL ANALYSIS OF BRITTLE FRACTURE (Unclassified)

12. PERSONAL AUTHOR(S)
T. J. Mackin and J. J. Mecholsky

13a. TYPE OF REPORT	13b. TIME COVERED	14. DATE OF REPORT (Year, Month, Day)	15. PAGE COUNT
MS Thesis	FROM _____ TO _____	October 1987	103

16. SUPPLEMENTARY NOTATION

17. COSATI CODES			18. SUBJECT TERMS (Continue on reverse if necessary and identify by block number)
FIELD	GROUP	SUB-GROUP	Fractal analysis, fractal geometry, fractal dimension,

19. ABSTRACT (Continue on reverse if necessary and identify by block number)

Fractal geometry provides a tool for the description of irregular objects. While Euclidean geometry allows for only integer dimensions, fractal geometry admits to the existence of a dimensional continuum. Thus, geometric shapes can be classified according to their dimensions.

In previous work, a relationship was shown to exist between a materials fracture toughness and its fractal dimension. It was found that:

20. DISTRIBUTION / AVAILABILITY OF ABSTRACT	21. ABSTRACT SECURITY CLASSIFICATION
☒ UNCLASSIFIED/UNLIMITED ☐ SAME AS RPT ☐ DTIC USERS	Unclassified
22a. NAME OF RESPONSIBLE INDIVIDUAL	22b. TELEPHONE (Include Area Code) 814/865-6344 / 22c. OFFICE SYMBOL

DD FORM 1473, 84 MAR — 83 APR edition may be used until exhausted. All other editions are obsolete.

SECURITY CLASSIFICATION OF THIS PAGE
Unclassified

$$K_{Ic} \sim (D-1)^{1/2},$$

where: K_{Ic} is mode I fracture toughness,

D is the fractal dimension .

Assuming that fracture can be modelled as a scaling fractal, the constant of proportionality of this relationship is found to be a product of Young's modulus (E) and a characteristic length (a_0);

$$K_{Ic} = A(D-1)^{1/2},$$

where $A = E(a_0)^{1/2}$.

The constant A is a family parameter which identifies a line in the toughness-fractal dimension plane. Materials within a given line experience an increase in toughness as the fractal dimension increases.

Using experimentally determined values of K_{Ic} , E, and D, a characteristic length, a_0 , can be computed. This length is indicative of the "unit process" of fracture, and represents an average step size in the geometry of fracture. For example, the characteristic length of a polycrystalline alumina (AD90) is 3 Å , suggesting the Al-O bond rupture as characteristic of the fracture. Alternatively, a zinc silicate glass ceramic (MS498#5) has a characteristic length of 76 Å. This indicates a cluster-like fracture, suggestive of glass-crystal molecular groupings as the unit process. Thus, if this model is correct, we have a technique whereby we can relate the geometry of the fracture surface of brittle materials to an atomic scale geometry.

ABSTRACT

Fractal geometry provides a tool for the description of irregular objects. While Euclidean geometry allows for only integer dimensions, fractal geometry admits to the existence of a dimensional continuum. Thus, geometric shapes can be classified according to their dimensions.

In previous work, a relationship was shown to exist between a materials fracture toughness and its fractal dimension. It was found that:

$$K_{Ic} \sim (D-1)^{1/2},$$

where: K_{Ic} is mode I fracture toughness,

D is the fractal dimension .

Assuming that fracture can be modelled as a scaling fractal, the constant of proportionality of this relationship is found to be a product of Young's modulus (E) and a characteristic length (a_0):

$$K_{Ic} = A(D-1)^{1/2},$$

where $A = E(a_0)^{1/2}$.

The constant **A** is a family parameter which identifies a line in the toughness-fractal dimension plane. Materials within a given line experience an increase in toughness as the fractal dimension increases.

Using experimentally determined values of K_{Ic} , E, and D, a characteristic length, a_0 , can be computed. This length is indicative of the "unit process" of fracture, and represents an average step size in the geometry of fracture. For example, the characteristic length of a polycrystalline alumina (AD90) is 3 Å , suggesting the Al-O bond rupture as characteristic of the fracture. Alternatively, a zinc silicate glass ceramic (MS498#5) has a characteristic length of 76 Å. This indicates a cluster-like fracture, suggestive of glass-crystal molecular groupings as the unit process. Thus, if this model is correct, we have a technique whereby we can relate the geometry of the fracture surface of brittle materials to an atomic scale geometry.

TABLE OF CONTENTS

CHAPTER

LIST OF TABLES

TABLE

LIST OF FIGURES

FIGURE

FIGURE

FIGURE

ACKNOWLEDGMENTS

Jack Mecholsky is enduring, forgiving, energetic, enthusiastic and a black belt (Tae Kwon Do). Dann Passoja is creative, brilliant, curious, inspirational and, also, a black belt (Shorin Ryu). They made every step of this process a uniquely enjoyable experience. My mentors were the best.

My parents have watched me change life tracks a half-dozen times, yet they have never faltered in their support. Three brothers, three sisters, three brothers-in-law, three sisters-in-law, seventeen nephews and nieces. Every one of them offering support. Thank you. My friends in the lab: Todd, Dave, William, Jill, Tom, Cindy, Armando, Bulent, Carol, Peter, Ken. Good minds, good people. Dave Artis showed me the Mac, gave me a place to write, listened, criticized, encouraged and understood. Chopper gave me peace at the ocean, good laughs, the space to dream and positive thinking. Jasna showed me Colorado, the Aspen Institute for Physics, Fermi Lab, Drasko, Stanka and a lot of patience. Special thanks to my committee members: Rob Pangborn and Richard McNitt. Their time and effort makes this thesis possible.

Indelible memories of incredible people. I'm lucky to count you as my friends.

Funding for this research was provided by the Naval Sea Systems Command through the Applied Research Laboratory Exploratory and Foundational Research Program.

CHAPTER 1

INTRODUCTION TO FRACTALS AND FRACTURE

Fractals

Fractal geometry is a non-Euclidean geometry that was developed, popularized and applied by B.B. Mandelbrot.[1,2] The word fractal is derived from the latin "fractus" which means fragmented or broken. Mandelbrot realized that fragmented geometries rather than Euclidean geometries are, by far, the most common geometries of nature. His research has created a framework for the description of systems that, up to now, were too chaotic for geometric description.

In his book, The Fractal Geometry of Nature, Mandelbrot describes the extensive applications of fractal geometry. The concepts have been used to describe the geometry of clouds, soot aggregates, dielectric breakdown, mountainous terrain, coastlines, etc. This thesis uses the notions of fractal geometry to describe the geometry of fracture surfaces.[3]

Basic Concepts of Measure

To establish a "feel" for fractal geometry we can simply consider how we measure the length of a line.[4] It is clear that the measurement of a set requires a measuring tool, or ruler.

Suppose we use a supply of discs of a given radius, R, and consider the line of Figure 1.

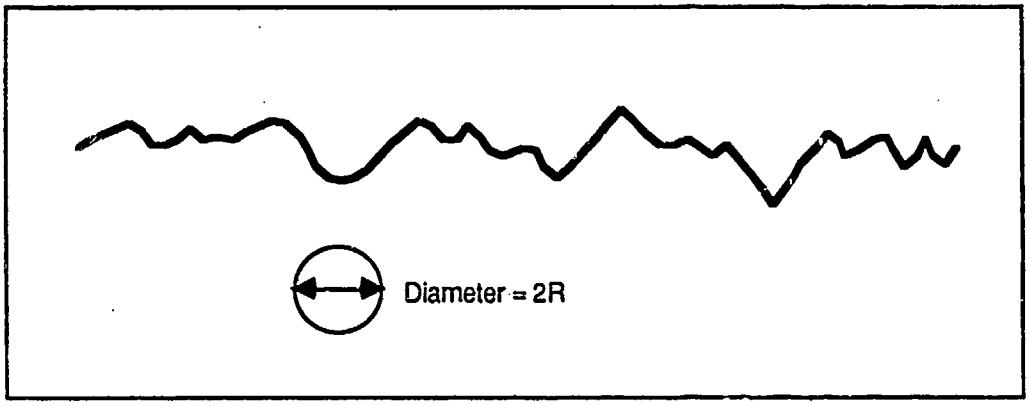

Figure 1. Measuring the length of a line requires a ruler

The length of this line is measured by covering it completely with as few discs as possible, as in Figure 2. The length, then, is given by:

$$\text{length} = (\text{number of discs}) \times (2R)$$

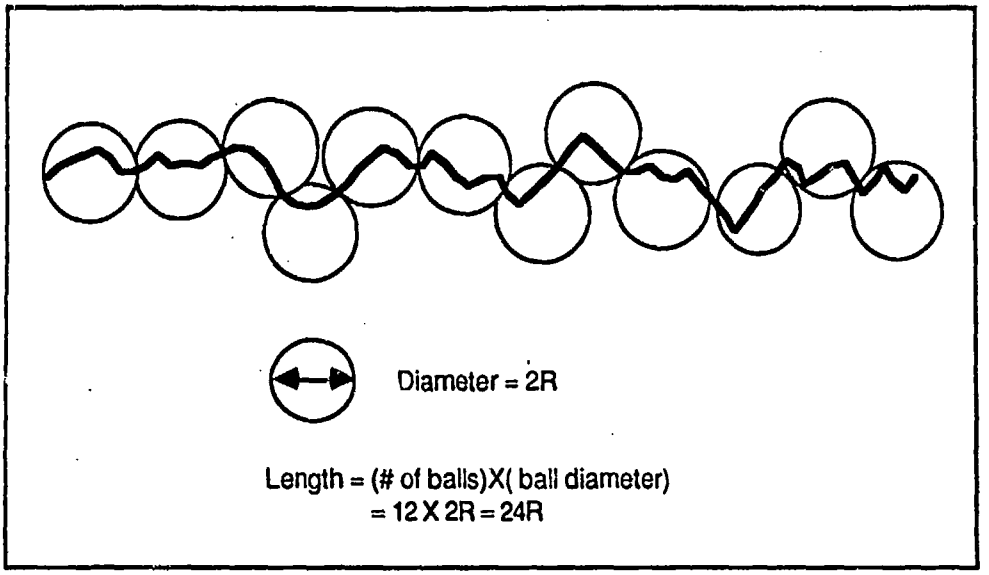

Figure 2. The line is completely covered to determine its length.

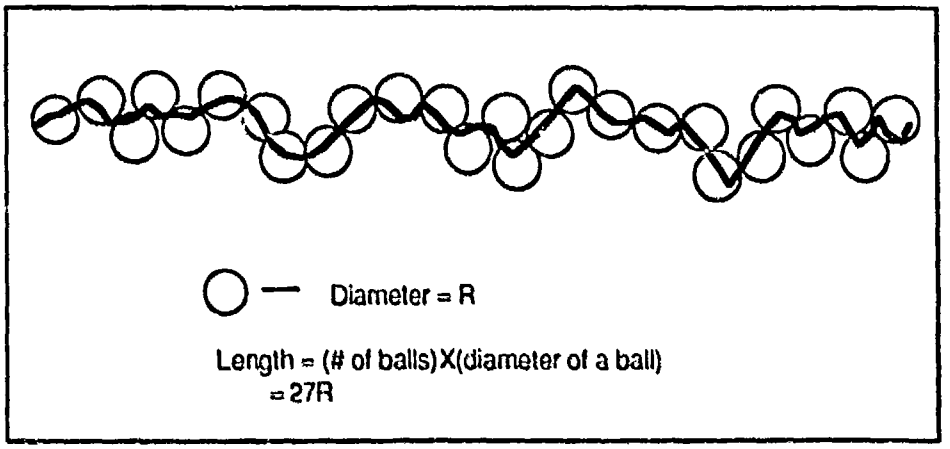

Figure 3. Changing the size of the measuring disc may produce a different measure of the length.

Now, suppose we have a new supply of discs with a different radius, say (1/2)R. The line length is determined in the same manner, and a new line length is computed, Figure 3. Note the difference in the measured line length in Figures 2 and 3. Although the measuring disc was decreased to half of the original measure, the number required to cover the line more than doubled. The "tortuous" nature of this curve gives a length that is scale dependent. As the scale decreases, the measured length increases.

The measured length of a line can be succinctly described by the following equation, called Richardson's equation[1]:

$$L = kE^{1-D}. \qquad (1)$$

Where; L is the measured length,

E is the measuring scale,

D is the dimension of the curve,

k is a proportionality constant.

If D is equal to one, the line is Euclidean and its measured length is not a function of scale. If $1<D<2$, the curve is said to be fractal with a dimension given by D. This dimension can be thought of as an indicator of the "wiggliness" or space filling nature of the curve.

If we are given a line, we can compute its fractal dimension from equation (1). The line's length is computed over a range of scales. A log-log plot of length vs. scale gives a straight line with slope equal to 1-D, Figure 4.

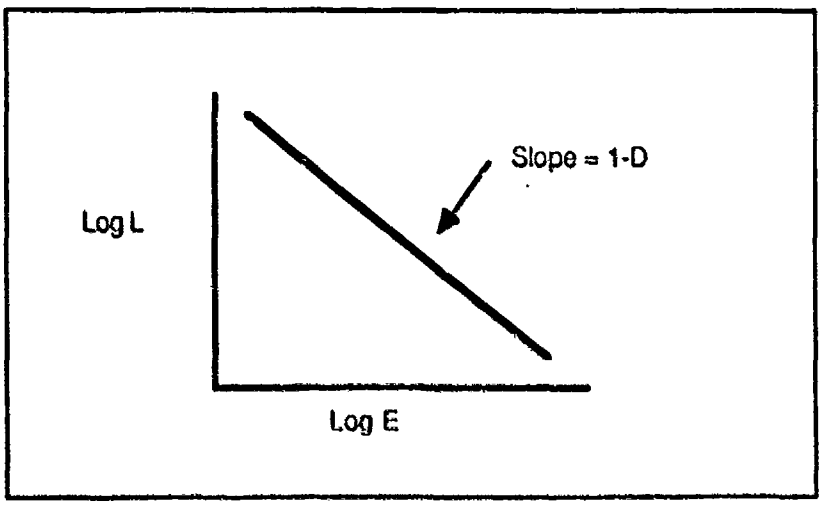

Figure 4. A log-log plot of Richardson's equation provides a slope equal to 1-D.

It should be mentioned that mathematical fractals will obey equation (1) for all scales. Thus, as the scale goes to zero, the measured length becomes infinite. Physical fractals, however, may have a finite cutoff at both the large and small scales. In the physical world, the fluctuation of a line will find its limit in the smallest measureable feature. The sensitivity of our measuring stick will determine the smallest feature we can measure. If fluctuations occur below the sensitivity of our instrument, the line will appear to be Euclidean. In this instance, the upper bound of the measured length of a line is simply that length that corresponds to the finest possible scale of measurement. We could not conclude, however, that the line has exhausted its fluctuation, we have simply exhausted our ability to measure any fluctuations.

On the contrary, a line may be composed of indivisible components. After our measuring stick has become smaller than the smallest of these components, the line would cease to exhibit scale-dependent length. This length, then, would represent a true upper bound. Such a line could be called "fractal" over the range it exhibited scale-dependent length. It is not, however, a fractal in the strict mathematical sense.

Both of the aforementioned possibilities would have a Richardson plot as in Figure 5. The object would be described as a fractal over a bounded range of scales. These cut-off scales are of special significance to the particular geometry of a specific physical phenomenon.

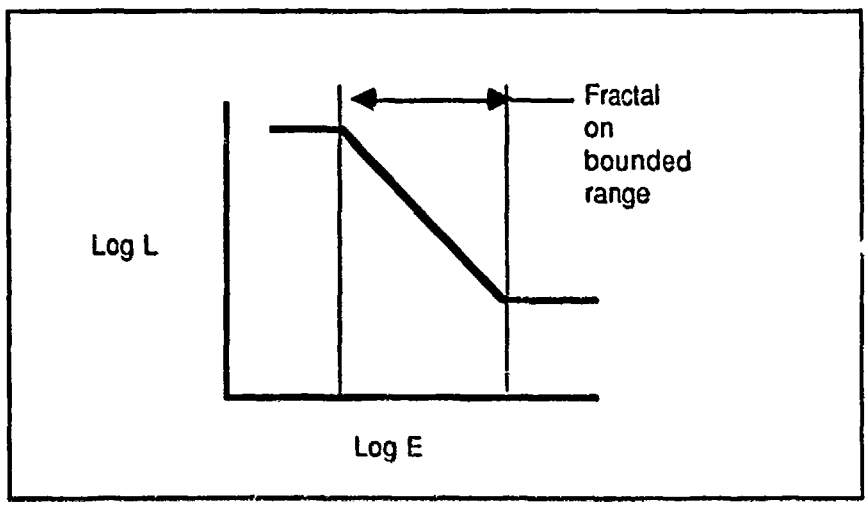

Figure 5. Physical fractals have scale dependence over a bounded range of scales.

Fractals and Fracture

Fracture markings on glasses and polycrystalline brittle materials (known as mirror, mist and hackle) are precursors to crack branching[5] and can be used to describe the stress state[6] and characteristics of crack propagation.[7] These markings have been observed for over 50 years and were related

quantitatively to the stress in the 1950's.[8] More recently, the repetition of these features (multiple mirrors) was observed and quantitatively related to stress intensity.[9] Ravi-Chandar and Knauss[5] also recently noted that mist and hackle are self-similar; i.e., they appear to be physically similar and produced in the same fashion. This observation follows previous detailed descriptions of the structure of mist and hackle.[10] These descriptions did not, however, emphasize the self-similar nature of the features. These recent observations of multiple mirror, mist, hackle, crack-branching and self-similarity led to this research.

A Basic Model of Fracture

In order to understand the essentials of material fracture, fracture mechanists employ a basic model of fracture. In this model, atoms interact with their nearest neighbors via a simple two-body potential. The derivation assumes that atoms lie in a plane, that they interact only with their nearest neighbor and that bonds break sequentially. That is, fracture is localized to only two atoms at a time.

The potential energy between atoms in a crystal structure can be approximated by a function of the form[11];

$$U = -Q_1 / r^x + Q_2 / r^y, \qquad (2)$$

where $-Q_1 / r^x$ is an attractive term,

Q_2 / r^y is a repulsive term.

For ionic crystals, the exponent in the attractive term (x) is close to unity while the repulsive exponent (y) is between 6 and 12. Such a function would have the form shown in Figure 6, where d_0 is the equilibrium spacing between neighboring atoms. The depth of the potential minimum is related to fracture energy, while the curvature of the potential minimum is an indication of the modulus. The derivative of this potential function gives the force function between neighboring atoms, as shown in Figure 7.

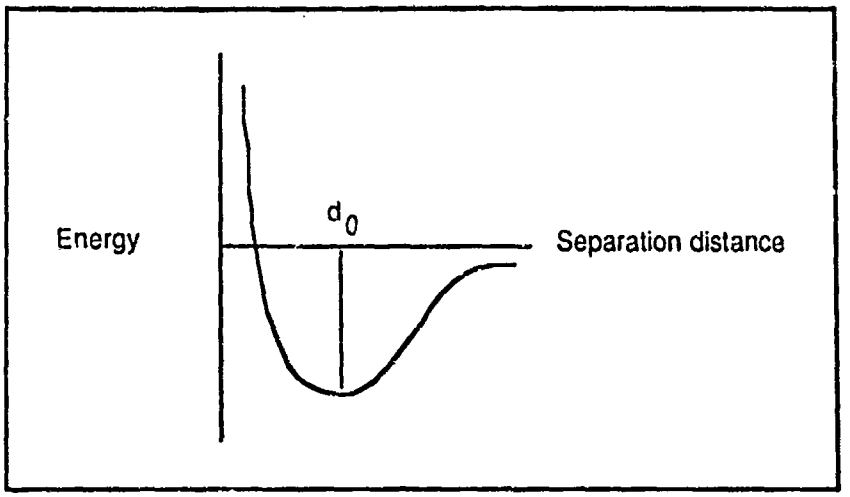

Figure 6. Potential energy between neighboring atoms

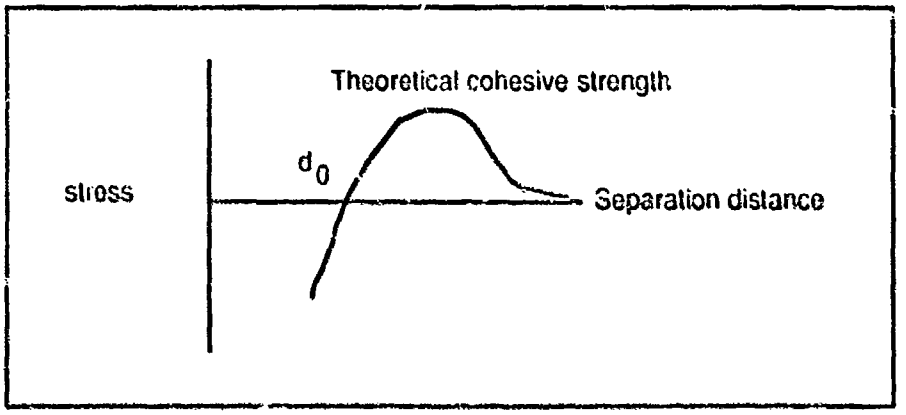

Figure 7. Force function between neighboring atoms.

When a material is stressed beyond a certain limit, irreversible changes will occur. If loading is continued, the material can be fractured. As a crack propagates through a specimen, the potential energy of the specimen is reduced.[12]

Energy is released via the creation of new surface, the emission of light, acoustic energy, etc. The energy required to propagate a crack is called the fracture energy, γ_f.

Crack propagation through a microstructure is a geometrically complicated statistical process that contains atomic scale as well as macroscopic scale geometries.[13] Interaction of the crack front with the microstructure will affect the geometry and, hence, the surface area generated.

A material's resistance to crack propagation is called fracture toughness. Fracture toughness may be characterized by the fracture energy, γ_f, the strain energy release rate, G_C ($G_C = 2\gamma_f$), or the critical stress intensity factor K_C ($K_C = \sqrt{2E\gamma_f}$). A toughening mechanism, then, is a microstructural property that affects a material's fracture toughness. One particular class of toughening mechanisms relies on influencing the direction of crack propagation (e.g., crack deflection[14]). An increase in toughness can be achieved by making the crack path irregular.[14] Thus, the geometry of the fracture surface plays a role in the material's toughness.

The importance of fracture energy is made obvious in the following simplified derivation assuming plane fracture in a perfect crystal.[11,15,16] A crack is assumed to reside between two planes of atoms with interplanar spacing d_0, Figure 8.

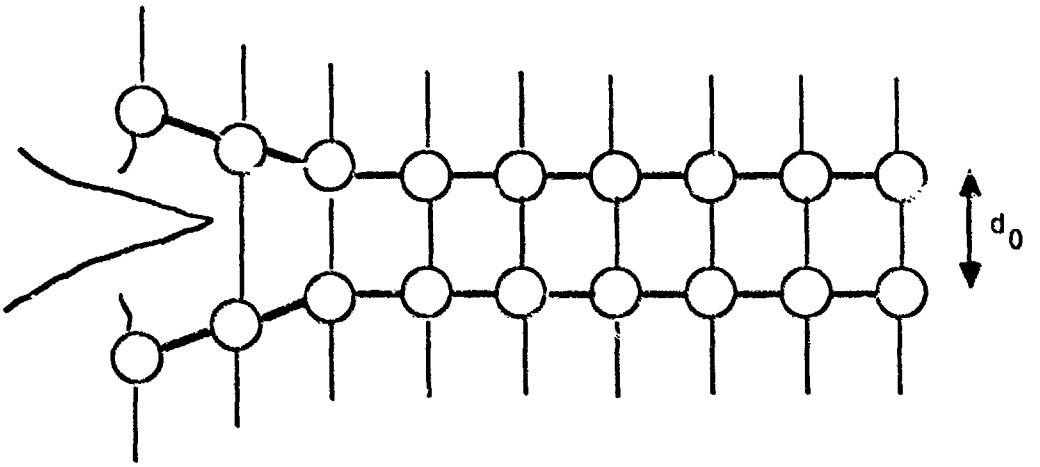

Figure 8. Idealized crack separating planes of atoms in a crystal structure.

Rather than using the derivative of equation (2), the stress resulting from the strain of the interplanar bonding is approximated by a sinusoidal function, Figure 9.

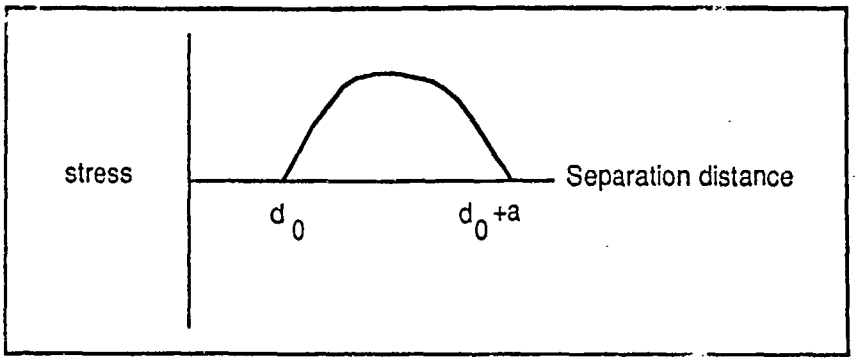

Figure 9. Sinusoidal approximation of the force between neighboring atoms.

At the equilibrium spacing, d_0, the stress is zero, rising to a maximum and dropping to zero at a distance d_0+a, the distance of bond rupture.

Therefore, $\sigma = \sigma_0 \sin(\pi(x-d_0)/a)$, (3)

where; x is the separation beyond equilibrium,

a is the failure separation.

For small displacements, x, the sin is equal to its argument.

Therefore, $\sigma = \sigma_0 \pi (x-d_0)/a$, (4)

and $d\sigma/dx = \sigma_0\pi/a$. (5)

By definition, the strain is;

$$\varepsilon = x/d_0 , \tag{6}$$

and, for small displacements,

$$\sigma = E\varepsilon = Ex/d_0 , \tag{7}$$

so that $$d\sigma/dx = E/d_0 . \tag{8}$$

Comparing equations (5) and (8) provides;

$$\sigma_0 = Ea/\pi d_0 . \tag{9}$$

Thus, an estimate of the theoretical cohesive strength is obtained from known values of E, a , and d_0. Now, in fracture, the work of separation must at least be equal to the energy required to create two new surfaces, $2\gamma_s$.[11,15,16]

The work per unit of area generated by fracture is;

$$\text{work/unit area} = \int \sigma_0 \sin\pi(x-d_0)/a \, dx = 2\gamma_s , \qquad (10)$$

so that,

$$2\sigma_0 a/\pi = 2\gamma_s , \qquad (11)$$

but, from equation (7);

$$2Ea^2/\pi^2 d_0 = 2\gamma_s . \qquad (12)$$

so

$$\gamma_s = Ea^2 / \pi^2 d_0 . \qquad (13)$$

Equation (13) shows that the surface energy for plane fracture, γ_s, is a function of modulus, E, interplanar spacing, d_0, and the displacement to bond rupture, a. For single crystals, the surface energy, γ_s, is assumed to be nearly equal to the fracture enrgy, γ_f. Gilman[16] assumed that the constant, a, was equal to the radius of atoms within a given plane.

For single crystals, his results were uniformly high, yet of the same order of magnitude as experimentally obtained values. Polycrystalline fracture energies, however, are approximately an order of magnitude higher than their single crystal counterparts.[11] Part of this difference is due to an increase in the roughness of the fracture surface.

The model of fracture presented here takes no account of fracture surface roughness. It is assumed that fracture creates two perfectly plane fracture surfaces. Fractal geometry can accommodate surface roughness by allowing for irregular paths. These paths could be constructed from straight line segments imbedded in an orderly geometric matrix.

Imagine a two-dimensional array of atoms as shown in Figure 10. Fracture could progress from region A to region B through a number of paths. Some of these paths are shown in the Figure (a-a, b-b, and c-c). The basic model would assume only a straight line, whereas a fractal model could describe other more complicated paths. Thus, surface roughness can be accommodated without a radical departure from the basic model.

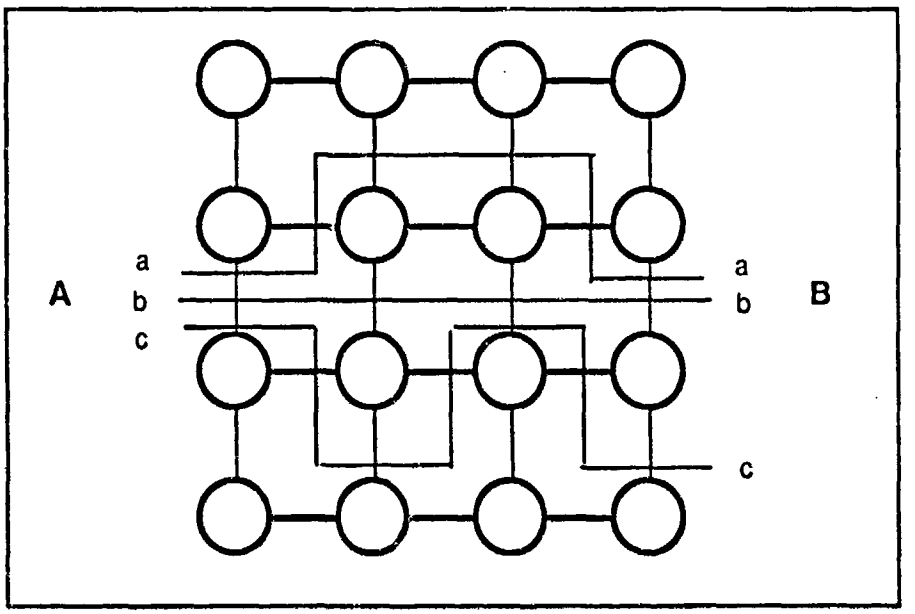

Figure 10. Schematic of possible crack paths in an idealized lattice.

Fracture Energy and Fracture Toughness

Equation (9) provides an estimate of the theoretical cohesive strength of a material. Brittle ceramics exhibit fracture strengths that are generally orders of magnitude lower than this estimate. This difference results from the stress concentrating effects of flaws.

Griffith[12] was able to calculate the stress at which a crack would propagate. He postulated that crack extension would occur only if the creation of new surface acts to reduce the potential energy of the system. He found that, under conditions of plane stress;

$$\sigma_f = (2E\gamma_f/\pi C)^{1/2}. \qquad (14)$$

Where: σ_f is the fracture strength,

E is Young's modulus,

γ_f is the fracture energy,

C is the flaw size.

Inglis made computations of the stress concentration created by flaws of various geometries. It was found that cracks in a material could be conveniently modelled as elliptical, and their stress concentration computed. The stresses near the tip of such elliptical cracks have a precise mathematical description that depends upon a parameter called stress intensity, K_I (The I denotes tensile loading). For a material to fail, the far field stress must be concentrated to the level of theoretical cohesive stress. Thus, stress intensity reaches a critical value called the fracture toughness, or critical stress intensity factor, K_{IC}. This critical value is found to depend on the flaw size and the far field stress;

$$K_{IC} = Y \sigma_f \sqrt{C}. \qquad (15)$$

Where: σ_f is the far field stress,

C is the flaw size,

Y is a factor that depends on the geometry of loading and crack configuration.

Comparing equations (14) and (15) provides a relationship between K_{Ic} and γ_f. Under conditions of plane stress;

$$K_{Ic} = (2E\gamma_f)^{1/2}. \qquad (16)$$

Fracture Profiles as Fractal Curves

In many cases, a fracture surface presents a rather complicated geometric structure. This complex geometric shape is not amenable to description by Euclidean geometry, thus, fracture surface energies have not been accurately modeled as functions of this geometry. Fractals, however, provide a tool for the description of such surfaces. At the very least, they can be used to quantify the surface roughness. A fracture profile presents a curve similar to that of Figure 11. The "complexity" of this profile can be categorized by its fractal dimension. As discussed earlier, Richardson's equation, where the profile length is measured for various scales, provides a method for determining the fractal dimension. Of course, a fracture surface is, at the very least, a two-dimensional object, but as a first step in categorization, it is worthwhile to compute the dimension of the profile, Figure 11.

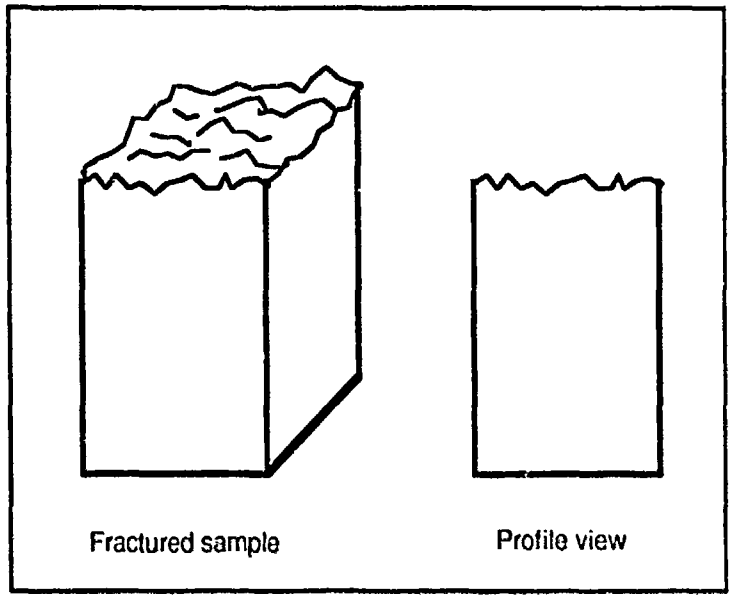

Figure 11. Fracture profiles can be measured according to Richardson.

It is quite possible that there will be a physical limit to the scale dependence of length. Features on the fracture surface may vary only down to a finite cut-off size. This may be on the grain size, molecular, or atomic scale. But, this, in itself, is useful information.

Scaling Fractals

There is a particular subclass of fractal geometry which is comprised of "scaling fractals".[1,3] This is what is generally referred to as a fractal. Regardless of the nature of a curve, Richardson's equation can be used to compute a fractal dimension. Scaling fractals, however, have two very important properties: scale invariance, and self-similarity. Scale invariance refers to features, geometrically identical, appearing on all scales of observation. Self-similarity means that a small feature of the object can be scaled to precisely match a large feature. These concepts are most easily understood by observing the construction of a scaling fractal.

Consider a box, as shown in Figure 12a[1,4,17], whose sides are of unit length. Next to this box is a shape called a generator, composed of line segments scaled to 1/4 of the length of a side of the box. Now, replace each side of the square with this "scaled" generator.

The result is shown in Figure 12b. Again, take the generator and scale it down to the length of each straight line segment of this new object. The generator is now composed of line segments of length $(1/4)^2$. Replace each of the straight line segments of Figure 12b with the scaled generator. A portion of the resulting shape is shown in Figure 12c. This process is continued, ad infinitum, generating an object which is said to be scale invariant and self-similar.

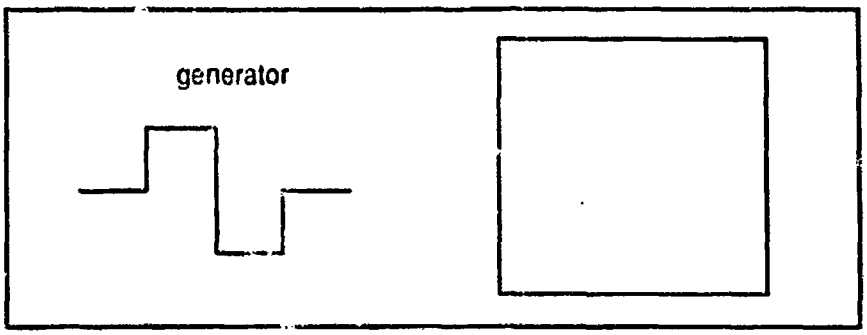

Figure 12a

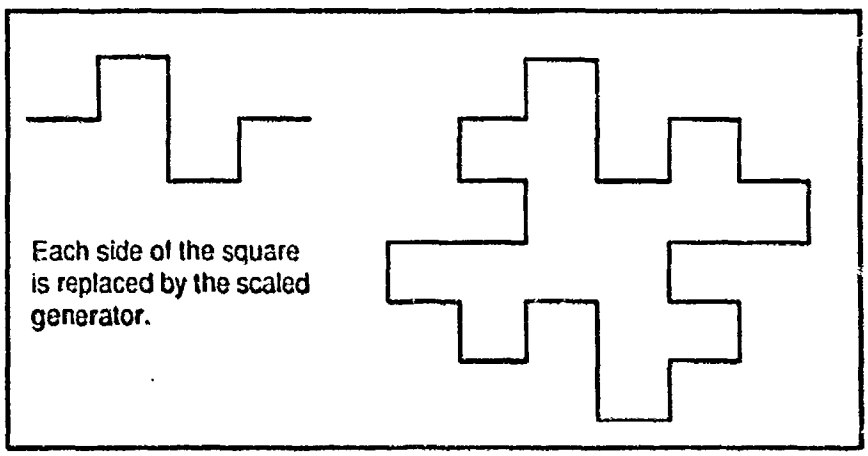

Figure 12b

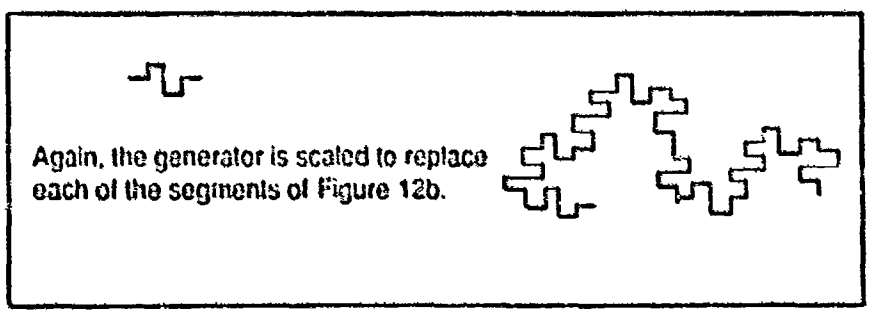

Figure 12c

Figure 12. The stepwise construction of a scaling fractal.

A scaling fractal looks geometrically the same everywhere and on all scales. Clearly, we have generated an object whose perimeter will be a function of scale (as in equation 1). The fractal dimension of this object, however, can be computed in another, quite different fashion.[1,4] Scaling fractals obey the following;

$$Nr^D = 1. \tag{17}$$

Where: N is the number of elements in the generator,
r is the scale factor of an element,
D is the similarity or fractal dimension.

For the curve of Figures 12, called the quadratic Koch curve, N = 8, r = 1/4. Thus,

$$D = \log 8 / \log 4 = 3/2. \tag{18}$$

Figure 13 contains three photographs of a glass fracture surface. Such fractures contain readily identifiable regions called mirror, mist, and hackle. A glance at the photographs will demonstrate the similarity of the mist and hackle regions.

Figure 13b is a photo of the mist-hackle boundary, while 13a is a view of the mirror-mist boundary. Figure 13c is a magnified view of a region in 13a. The identification of these boundaries is clearly affected by magnification. Given such scale dependence, it seems possible that a geometry that describes one region may simply be a scaled version of a geometry that describes another region. This is precisely the notion of scaling fractals and fractal geometry.

It is certainly true that fracture profiles can be measured according to Richardson's equation and, if such is the case, assigned fractal dimensions. The proposal of this thesis is that fracture surfaces can be accurately modelled as scaling fractals. Thus, we can imagine a scheme of generation and a generator that is repeated and scaled as fracture progresses. This generator may be an atomic scale process that cascades, through the scale invariance of fractal geometry, to the macroscopic features of a fracture surface. Given D, we can use equation 14 together with knowledge of the crystal structure of a material to determine possible values for r and N. Modelling fracture in this fashion allows for geometric interpretation of measurements on the macroscopic scale, to a description of geometry on the atomic scale.

Research has shown a relationship between fracture toughness (i.e., resistance to crack growth) and fractal dimension.[18,19,20,21,24] At first glance, this may not seem surprising. After all, fracture toughness is, in some ways, related to surface roughness, and fractal dimension provides a measure of this roughness. The relationship is not simple, however, and contains some interesting results.

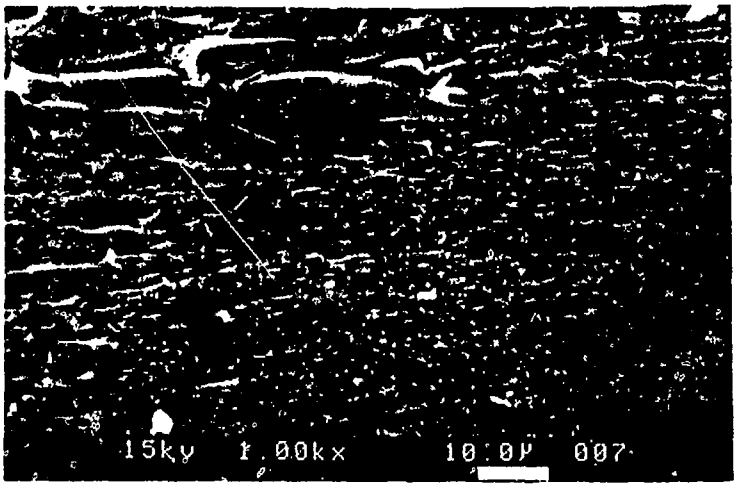

13a. Mirror-mist transition.

13b. Mist-hackle transition.

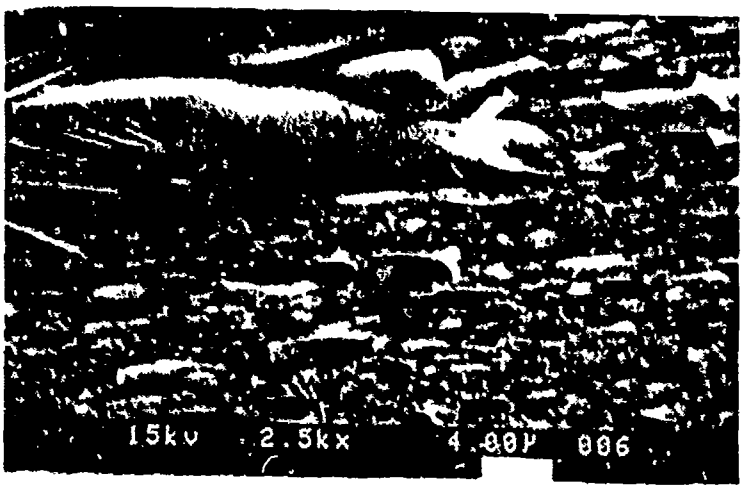

13c. Enlargement of the mirror-mist transition region.

Figure 13. Self-similarity of mirror, mist and hackle.

CHAPTER 2

EXPERIMENTAL TECHNIQUE

In this study, two independent techniques were used to determine the fractal dimension of fractured samples: slit-island analysis[19,22] and Richardson plots. Passoja[23] used a third technique, Fourier transform analysis, on a zinc silicate glass ceramic and obtained values within 2% of those obtained by slit-island analysis and Richardson plots.

Slit-Island Analysis

Fractured samples, obtained from previous studies,[6,7] were carefully cleaned and coated with nickel. The nickel coating performs two functions: It provides good contrast during polishing, and it helps to hold the fracture surface together. The samples are then potted in epoxy and polished parallel to the fracture surface,[19,22] Figure 14. As the fracture surface is encountered, a section of the fracture surface appears in the polishing plane. These sections appear as islands in the polishing plane. As polishing proceeds these islands begin to grow. The perimeter of the islands presents a line that can be measured according to Richardson's equation.

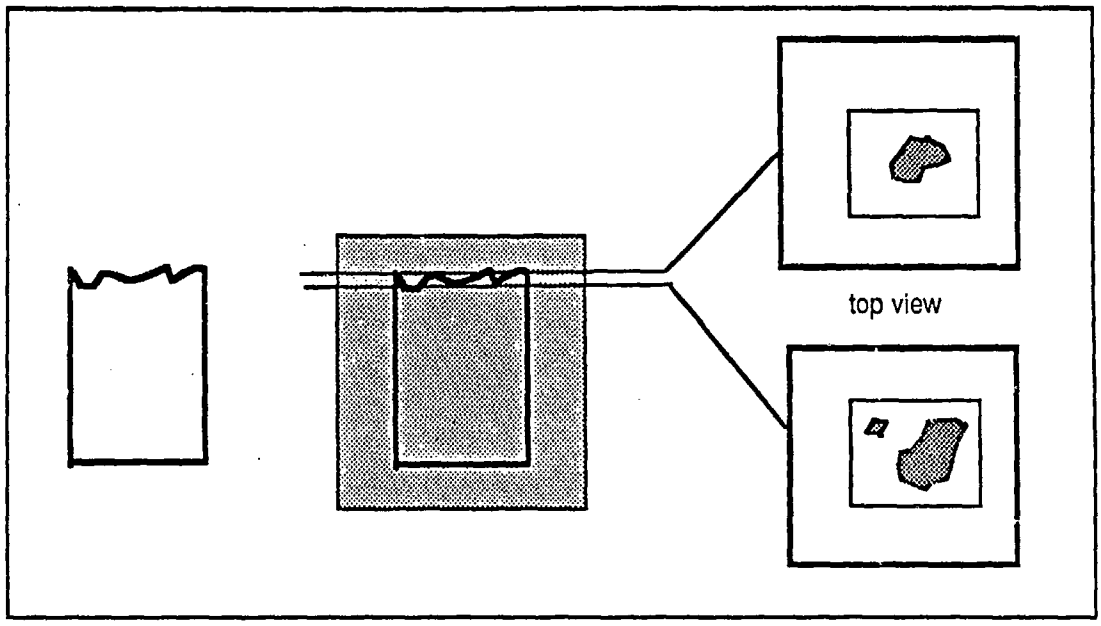

Figure 14. Fractured samples are encapsulated in epoxy and polished parallel to the fracture plane. Islands emerge in the polishing plane.

An adaptation of Richardson's equation reveals a relationship between the area and perimeter of an island;

$$A \sim P^{2/D} \tag{19}$$

where; A is the island area,

P is the island perimeter,

D is the dimension of the perimeter.

At the first emergence of an island, a polaroid photograph is taken at magnifications ranging from 10X to 400X. Polishing proceeds in stages, each stage followed by a photograph. Once a magnification is chosen, that same magnification is used for all subsequent photos. As polishing progresses, the islands grow and sometimes merge. A representative sequence of photos, taken at 10X magnification is shown in Figure 15. These photos are of a zinc silicate glass ceramic (MS-508).

The "roughness" of the perimeter is an indication of the roughness of the fracture surface. A sequence of approximately 20 photographs is taken to document island growth. These provide data for a log-log plot of area vs. perimeter (equation 19), from which a slope of 2/D is obtained. A representative graph is shown in Figure 16. Data and graphs for the materials tested are contained in following sections.

Photo #4

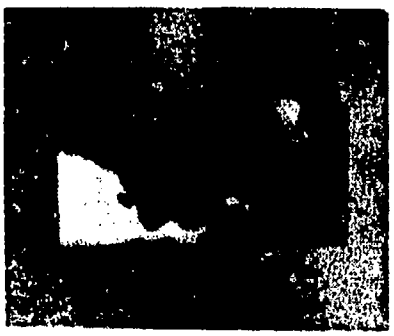

Photo #6

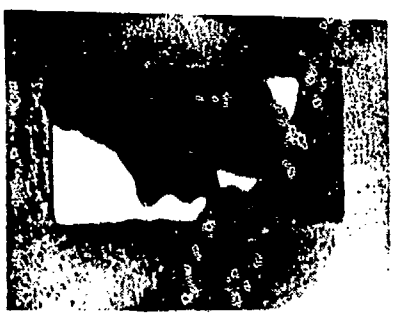

Photo #7

Photo #8

Figure 15. Sample photographs from zinc silicate MS508 slit-island analysis.

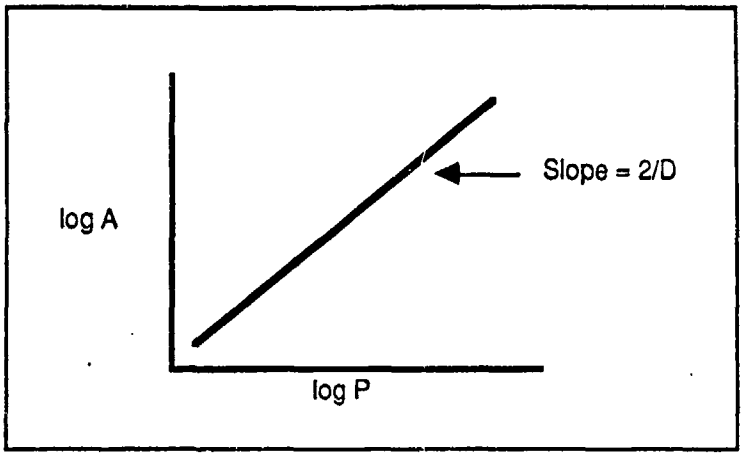

Figure 16. Fractal dimension can be obtained from area-perimeter growth of slit-islands.

Occasionally, an island will encounter the machined edge of a sample, (e.g., Figure 15). The island will have a perimeter that is composed of two sections: A line representative of the fracture surface, and a line representative of the machined edge. The resulting fractal dimension would be a weighted average of these two portions. Yet, our interest is only in that portion that represents the fracture surface. Such edge encounters are simply folded out of existence. Figure 17 explains graphically how the island can be folded across the edge to create an island with twice the original area and twice the "fracture perimeter." Thus, we are left with an island that is unbiased by the dimension of the sample edge.

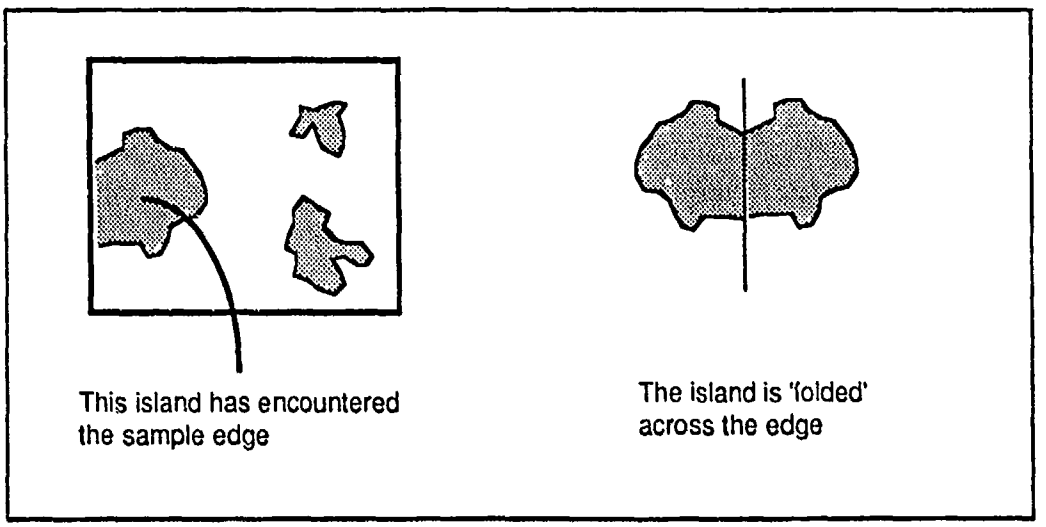

Figure 17. Edge correction is accomplished by simply folding an island across the sample's edge.

Island areas and perimeters are computed from the polaroid photographs using a Lemont Scientific image analysis system.[19] Different grey levels of the photographs are assigned different colors. The system software is then able to compute area and perimeter of the different colored regions.

In brief, the system places a grid with one micron spacing atop the selected image. Points of intersection of the grid and island perimeter are then assigned Cartesian coordinates. Straight lines are drawn between these points and simple trigonometry allows for the computation of the length of these lines. The island perimeter is taken to be the sum of these straight line segments. Island area is equal to the area of all totally enclosed rectangles plus the triangular regions along the edges. Figure 18 demonstrates this procedure.

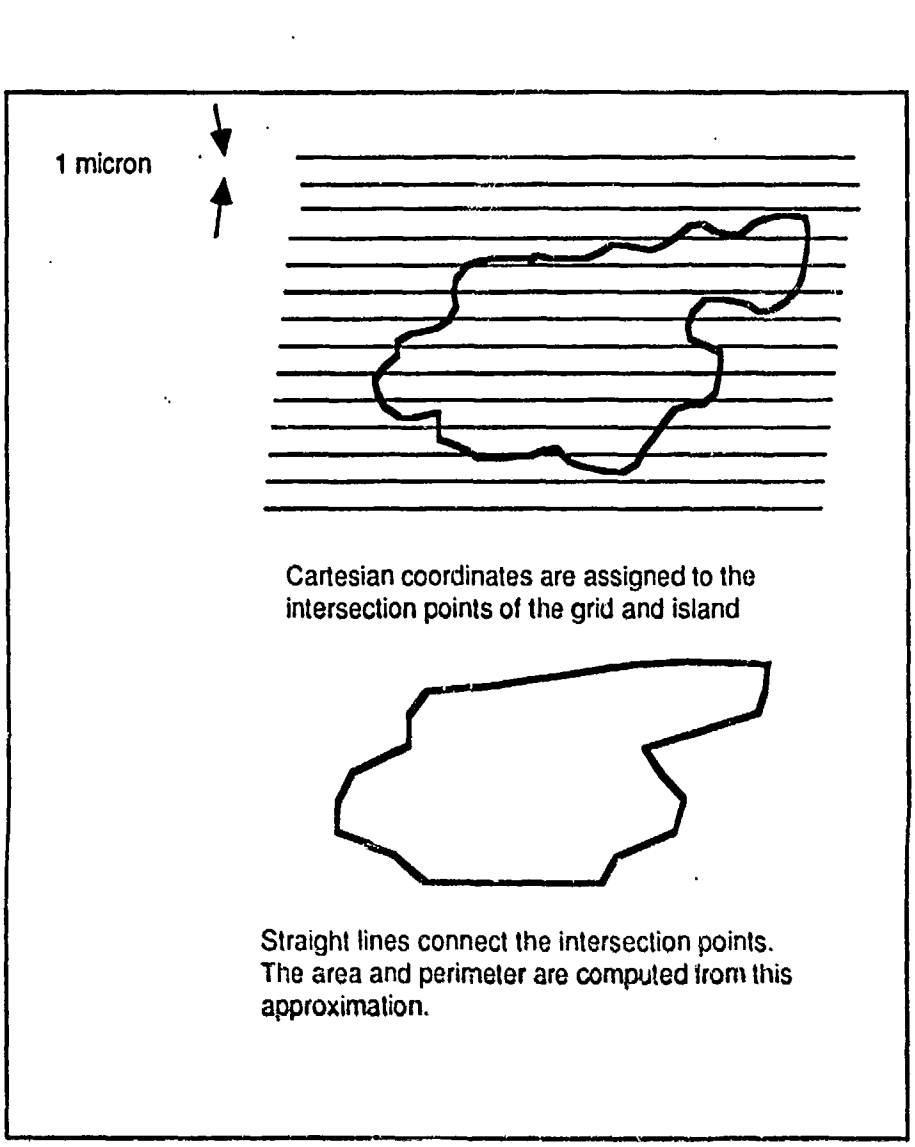

Figure 18. A grid is placed atop the island of interest. Intersection points of the grid and perimeter are used to compute area and perimeter.

The area and perimeter information is used to plot a graph for each island that appears on the fracture surface. Log-log plots, as in Figure 16, are used to extract the fractal dimension.

As a check on the entire procedure, an object of known dimension was analyzed with the slit-island technique. The chosen object was an alumina sphere. Any cutting plane through a sphere reveals a circle, the dimension of which is equal to one. The sphere was nickel coated, encapsulated in epoxy and polished. Sections through the sphere were photographed at 10X, Figure 19, and image analyzed. The results are shown in Figure 20. The computed dimension was equal to .98, a difference of only 2 percent from the expected value of a perfect sphere, D=1.0.

Photo #1

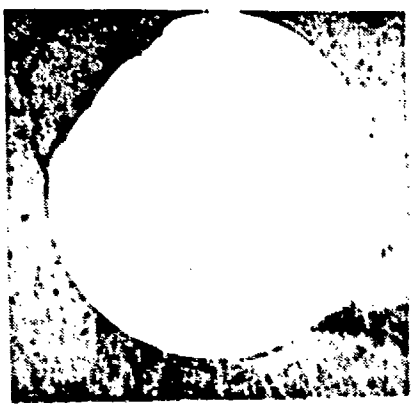

Photo #10

Figure 19. S[illegible]ple photographs from slit-island analysis of an alumina sphere.

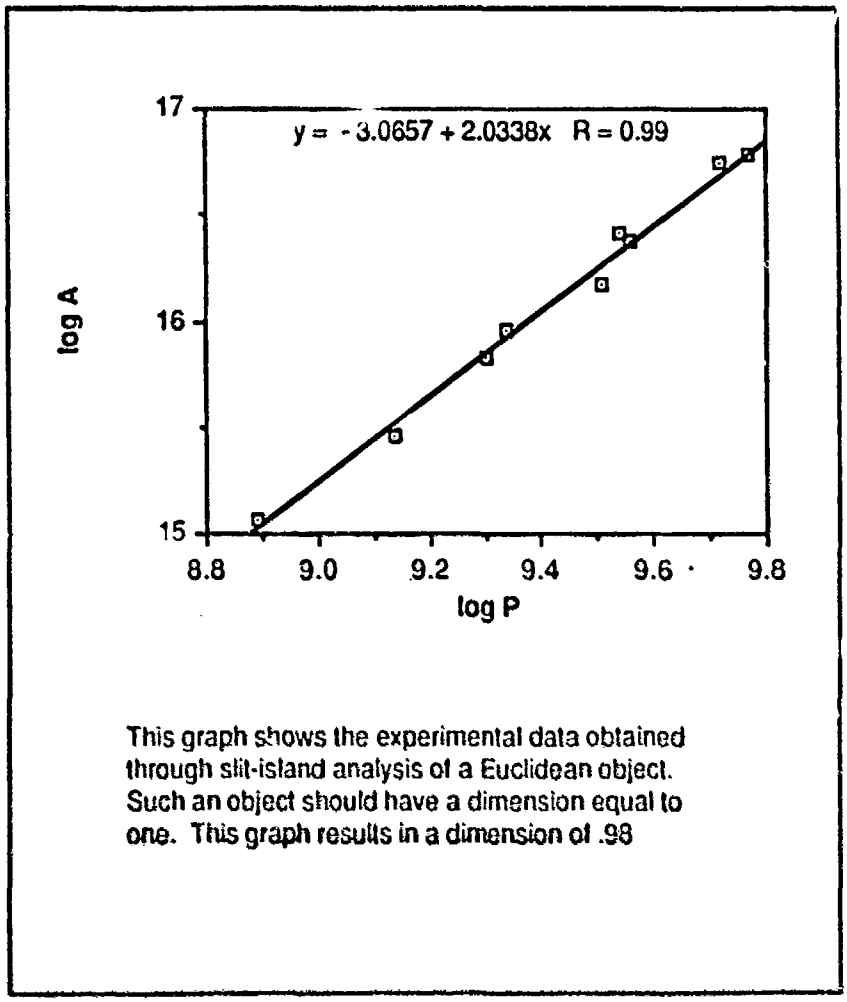

Figure 20. Data from the Euclidean test specimen.

Richardson Plot

Richardson plots, as mentioned in the introduction, detail the change in measured length of a line as a function of scale. Therefore, construction of a Richardson plot for a fracture surface requires a line that is representative of the fracture surface and a range of scales for measuring that line. As in slit-island analysis, fractured samples are coated with nickel and encapsulated in epoxy. The sample is then polished either parallel or perpendicular to the fracture plane. If polished parallel, we obtain an island whose perimeter is representative of the fracture. If polished perpendicular, we obtain a fracture profile. In either case a photo montage is constructed from polaroid photographs at 400X magnification. This montage is then measured with dividers set to 2, 1/2, 1/4, and 1/8 mm openings, as depicted in Figure 21. The length of the profile (or perimeter) is tabulated for each divider setting. In this fashion, profile length is computed as a function of scale. A log-log plot of length vs. scale (Figure 4) gives a straight line with slope equal to 1-D.

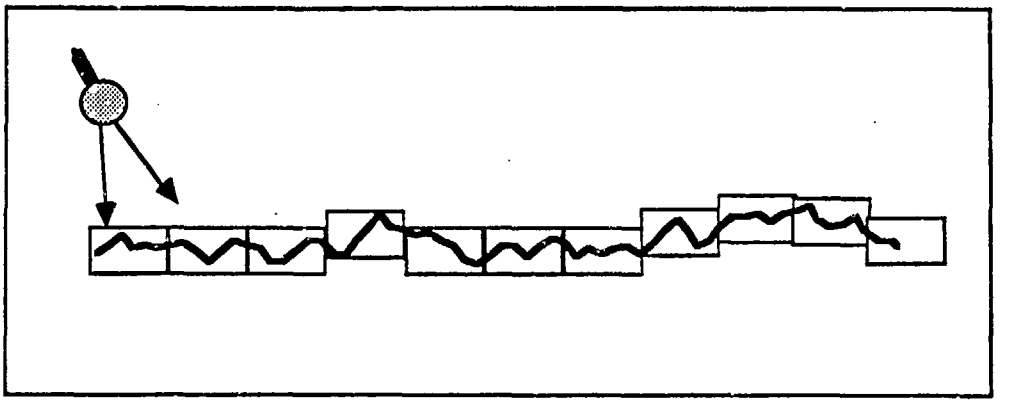

Figure 21. A montage of the profile is measured with dividers

The scale (or divider opening) is a measure of discernibility. The smallest observable feature is that of the scale. As the scale becomes finer, we observe greater and greater detail. If the scale is larger than the largest features, the observation is insensitive to those features. Thus, a curve will begin to look fractal only after the scale becomes smaller than such features. Figure 22 shows a sample montage for a section of island perimeter of an Ocala chert (chert U5).

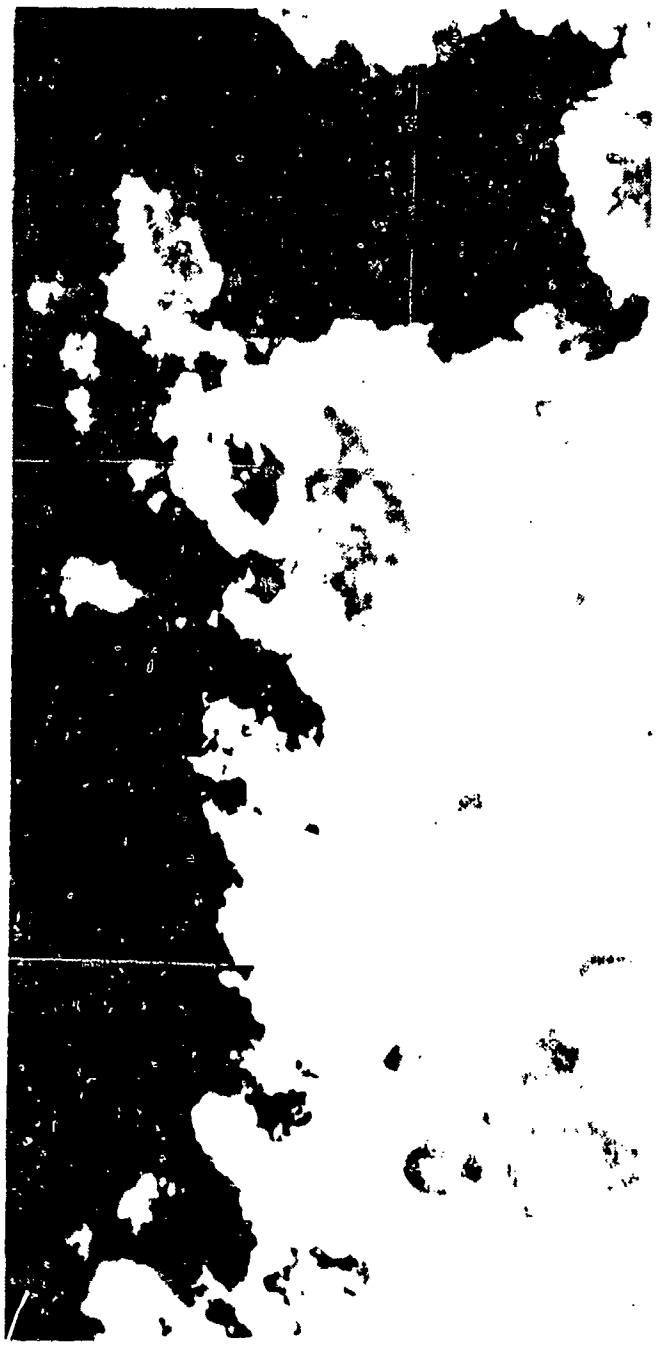

Figure 22. Sample island perimeter at 400X magnification.
This is a U5 chert sample, D = 1.32

CHAPTER 3

RESULTS AND DISCUSSION

Mecholsky, Feinberg and Passoja[24] determined a relationship between fracture toughness (K_{Ic}) and fractal dimension (D). They found that;

$$K_{Ic} \sim (D-1)^{1/2}. \qquad (20)$$

Thus, as fractal dimension increases, fracture toughness increases. (The term (D-1) will, henceforth, be referred to as D* . D* , then, is the fractional part of the fractal dimension). They obtained the fractal dimension of a number of zinc silicate glass ceramics and aluminas, Table I, Figure 23. The data conformed to a straight line in the log-log plane with a correlation of .92 .

A number of new materials were chosen for testing. A complete summary of these materials, the technique used for the determination of their fractal dimension, and the resulting fractal dimension is contained in Table II. A complete listing of the individual data tables and graphs follows this section.

The Ocala cherts, commonly referred to as flint, are similar in structure to glass ceramics (crystallites imbedded in an amorphous matrix). These cherts represent a series of heat treatments that alter the fracture toughness and fracture surface topography.

U5 chert was untreated and exhibits the highest toughness. Numbers three, four and F5 chert were heat treated at 300C, 400C, and 500C[25] respectively.

It is common to assume that fracture in single crystals will occur along a single plane. In general, loading conditions and inherent flaws will alter the planar propagation of a crack through such crystals. It is not certain, then, that the dimension of the fracture surfaces of single crystals will always be equal to one (plane fracture). Single crystals of Calcium Fluoride and Spinel were chosen to demonstrate this possibility. Large grain (~500μm) CdTe and ZnSe were dimensioned as a first step in determining grain size effects on the fractal dimension. Pyroceram 9606, a magnesium-aluminosilicate material, and MS508 Zinc Silicate are glass ceramics.

TABLE I

Data from Mecholsky, Feinberg and Passoja[19,24]

Material	Fracture Toughness K_{Ic} (MPa $m^{1/2}$)	Fractal Dimension
MS 498 6b #4	1.6	1.05
MS 500 12b #5	1.8	1.09
MS 500 #5	2.2	1.11
MS 498 #5	2.0	1.16
LAS glass ceramic	2.7	1.18
Monsanto Al_2O_3	3.5	1.21
GE Al_2O_3	3.9	1.23
Lucalox	4.0	1.31

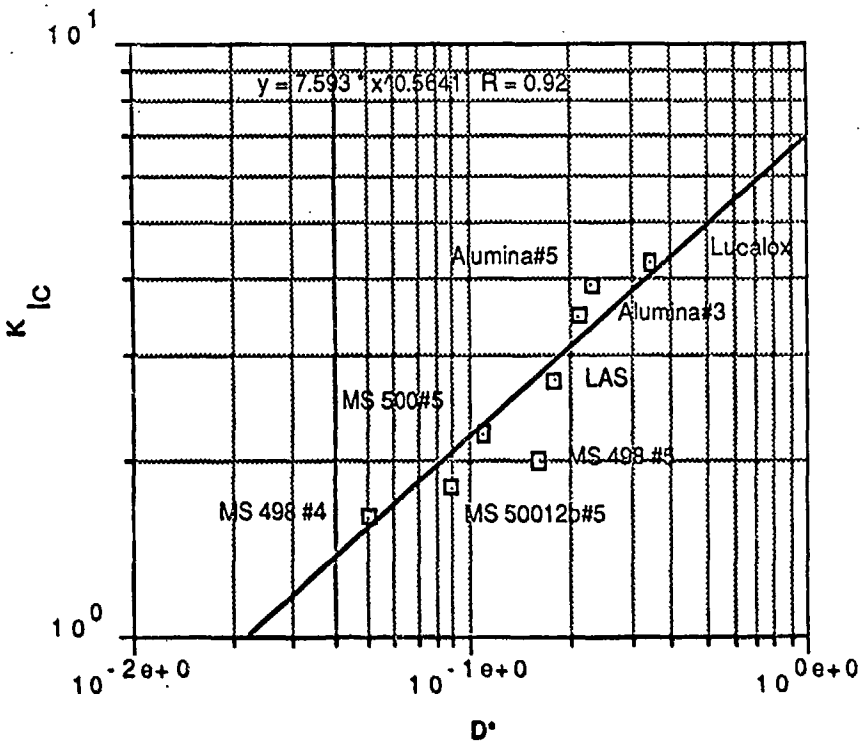

Figure 23. A graph of the data of Table I shows; $K_{Ic} \sim D^{*1/2}$.

TABLE II

Data Summary

Material	Fracture Toughness $MPa\,m^{1/2}$	Fractal Dimension	Measurement Technique
CdTe	.7	1.2	S.I.
ZnSe	.9	1.3	S.I.
PZT	1.5	1.23	R
MS 498	1.6	1.05	S.I.
MS 500#4	1.8	1.09	S.I.
MS 500#5	2.2	1.11	S.I.
MS 498#5	2.0	1.16	S.I.
Alumina #3	3.5	1.21	S.I.
Alumina#5 GE	3.9	1.23	S.I.
Alumina#3 GE	3.9	1.06	S.I.
Pyroceram	2.4	1.17	S.I.
Spinel(s.c.)	1.2	1.09	S.I.
CaF_2 (s.c.)	.3	1.07	S.I.
Poly Spinel	2.1	1.13	S.I.
U5 chert	1.55	1.32	R,S.I.
#3 chert	1.46	1.26	R
#4 chert	1.25	1.24	R
F5 chert	1.05	1.17	R,S.I.

*S.I. refers to the slit-island measurement technique, R refers to Richardson's technique

s.c. is a single crystal sample

Analysis of these new materials, at first glance, seemed to indicate no definite relationship between fractal dimension and fracture toughness. Indeed, as shown in Figure 24, the data is thoroughly scattered in the K_{Ic}-D^* plane. If, however, we assume that the relationship of Equation 20 is correct, we can order the data.

PROPOSITION: There exists a family of lines in the log-log K_{Ic}-D^* plane all of slope 1/2.

A graphical representation of this proposition is shown in Figure 25. Though we have no mathematical proof of this proposition, we may be able to demonstrate "reasonableness."

The existence of these curves implies a relationship between the points within any given line. Such points constitute a family and will be characterized by a family parameter. Any one of these lines will have the following functional form;

$$K_{Ic} = AD^{*1/2}, \qquad (21)$$

where; A is a family parameter.

The family parameter, **A**, identifies a line in the K_{Ic}-D^* plane. Within a family, an increase in fractal dimension corresponds to an increase in fracture toughness.

A vertical line in the K_{Ic}-D^* plane will intersect a number of family lines. Hence, materials which exhibit the same fractal dimension do not necessarily have the same toughness. Similarly, materials of equal toughness do not necessarily have the same fractal dimension. Thus, the functional relationship of Equation (21) is useful only in the comparison of materials within the same family.

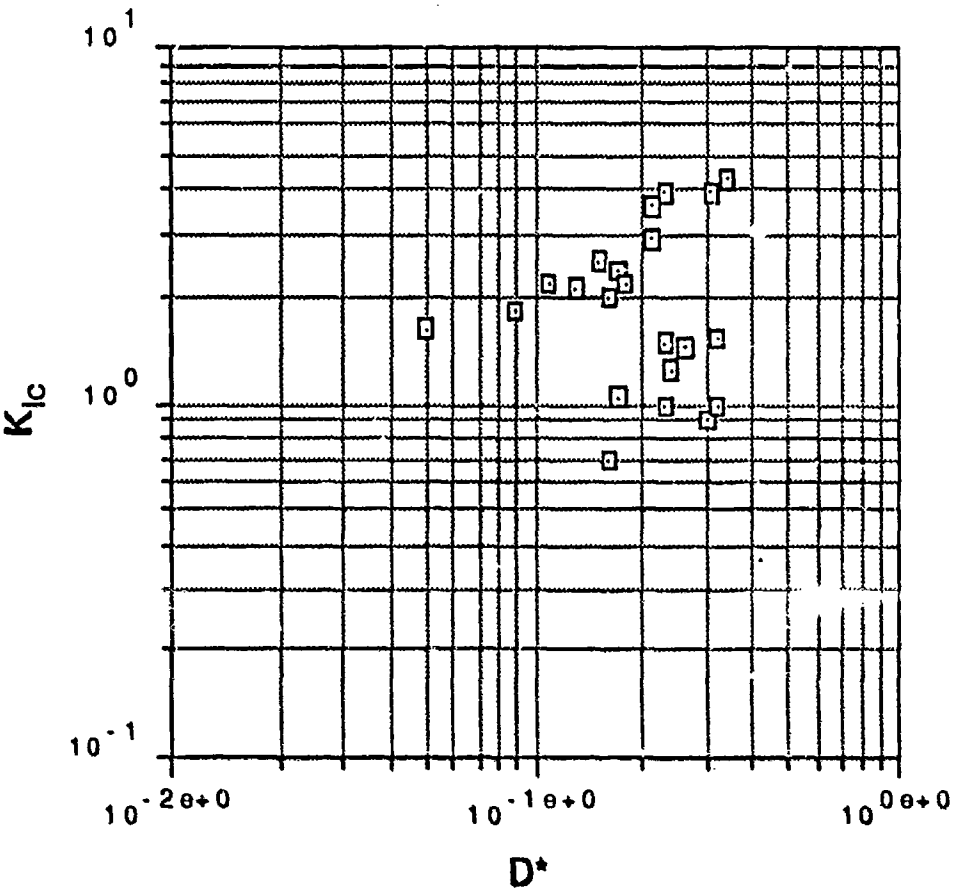

Figure 24. The data are apparently scattered in the K_{Ic}-D* plane

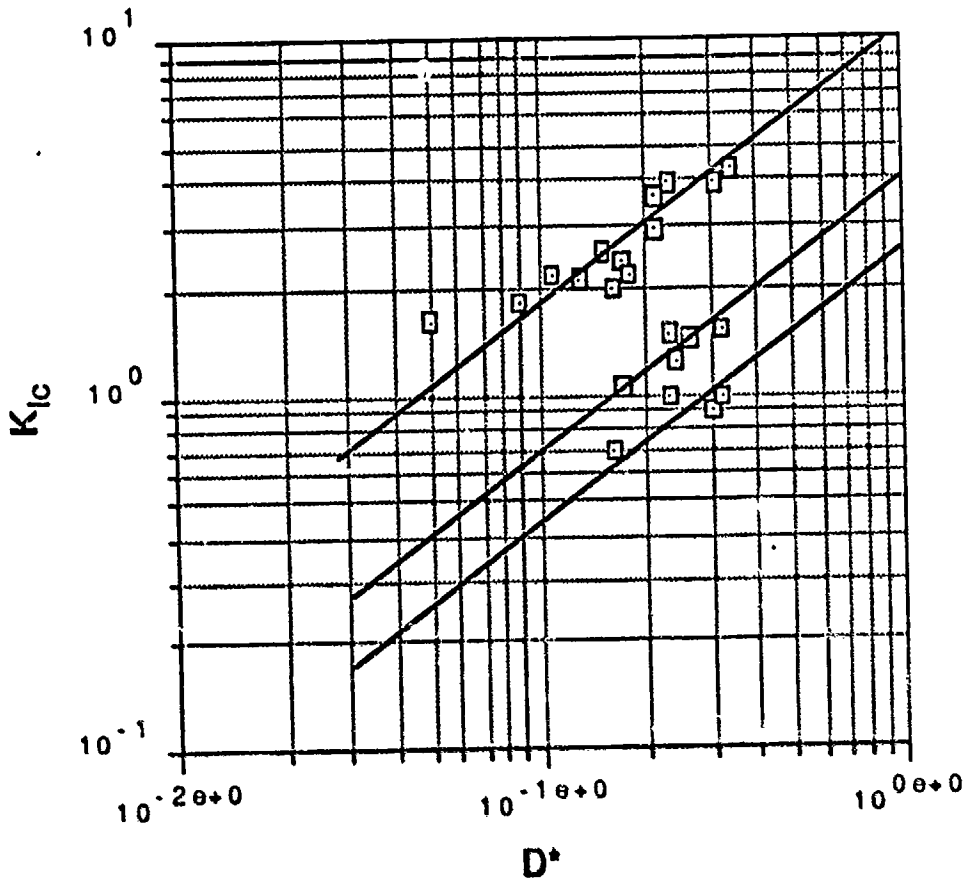

Figure 25. Family lines in the K_{Ic}-D* plane.

The Toughness-Fractal Dimension Relationship

As noted previously, toughness is proportional to fractal dimension;

$$K_{Ic} \sim D^{*1/2}. \tag{22}$$

The parameter which will identify a family in this space is the constant of proportionality, **A**;

$$K_{Ic} = AD^{*1/2}. \tag{23}$$

Since D^* is dimensionless, a dimensional analysis of this equation requires that **A** have the dimensions of toughness. Suppose that this constant can be further reduced to one involving Young's modulus, an indicator of bond strength, and some characteristic length parameter. The rationale for this supposition stems from the special importance attributed to scaling fractals. Scaling fractals are constructed from a unit process; i.e., a generator-shape which is scaled according to a scheme for generation. Thus, the geometry of fracture, if it can be accurately modeled by scaling fractals, will have such a unit process.

We propose that the fracture topography, in its atomic form, is recorded on the fracture surface through the scaling cascade of fractal geometry. There will, then, be an atomic scale generator with a characteristic length. Suppose the constant **A** is a product of this characteristic length and Young's modulus, so that $\mathbf{A} = E(a_0)^{1/2}$.

Then;

$$K_{Ic} = E\,(a_0 D^*)^{1/2}, \qquad (24)$$

where: K_{Ic} is the fracture toughness,

E is Young's modulus,

D^* is the fractal dimension,

a_0 is the characteristic length.

The plane fracture model of Chapter 1 demonstrated the importance of thermodynamic surface energy, γ_s, in fracture. This derivation assumed ideal plane fracture. The real world, however, is far from ideal. Other processes will absorb energy, the most obvious of which is the non-planar propagation of a crack. A new quantity, called the fracture energy, γ_f, is used as an effective fracture energy.

This term includes processes that consume energy by the formation of surface, zones of plastic deformation, acoustic and photo emission, etc.

Under conditions of plane stress, fracture toughness is related to fracture energy;

$$K_{Ic} = (2E\gamma_f)^{1/2}, \tag{25}$$

so that

$$K_{Ic}^2 = 2E\gamma_f. \tag{26}$$

Where; γ_f is the fracture energy.

Now, from equation 23;

$$K_{Ic}^2 = E^2 a_0 D^*. \tag{27}$$

Inserting equation 27 into equation 26 gives:

$$(\gamma_f / E) = 1/2\ a_0 D^*. \qquad (28)$$

Equation (28) can now be used to compute the value of a_0. Using experimentally obtained values of γ_f and E, and the experimentally determined value of D, a plot of (γ_f/E) vs $(a_0 D)$ is constructed, Figure 26. This plot is derived to have a slope of 1/2. The materials that were scattered throughout the K_{Ic}-D^* plane of Figure 25 are now situated along a single line.

The macroscopic fracture energy, γ_f, is normalized to Young's modulus, E. Young's modulus can be conceptualized as a measure of atomic bond strength. It represents a weighted average of all the possible bond strengths of the material. Thus, as γ_f/E increases, the fracture energy is increasing with respect to E. Along the horizontal axis, a_0 represents an atomic scale length while D^* represents a measure of surface roughness. Moving outward along this axis demonstrates another interplay between microscopic (a_0) and macroscopic (D^*) properties.

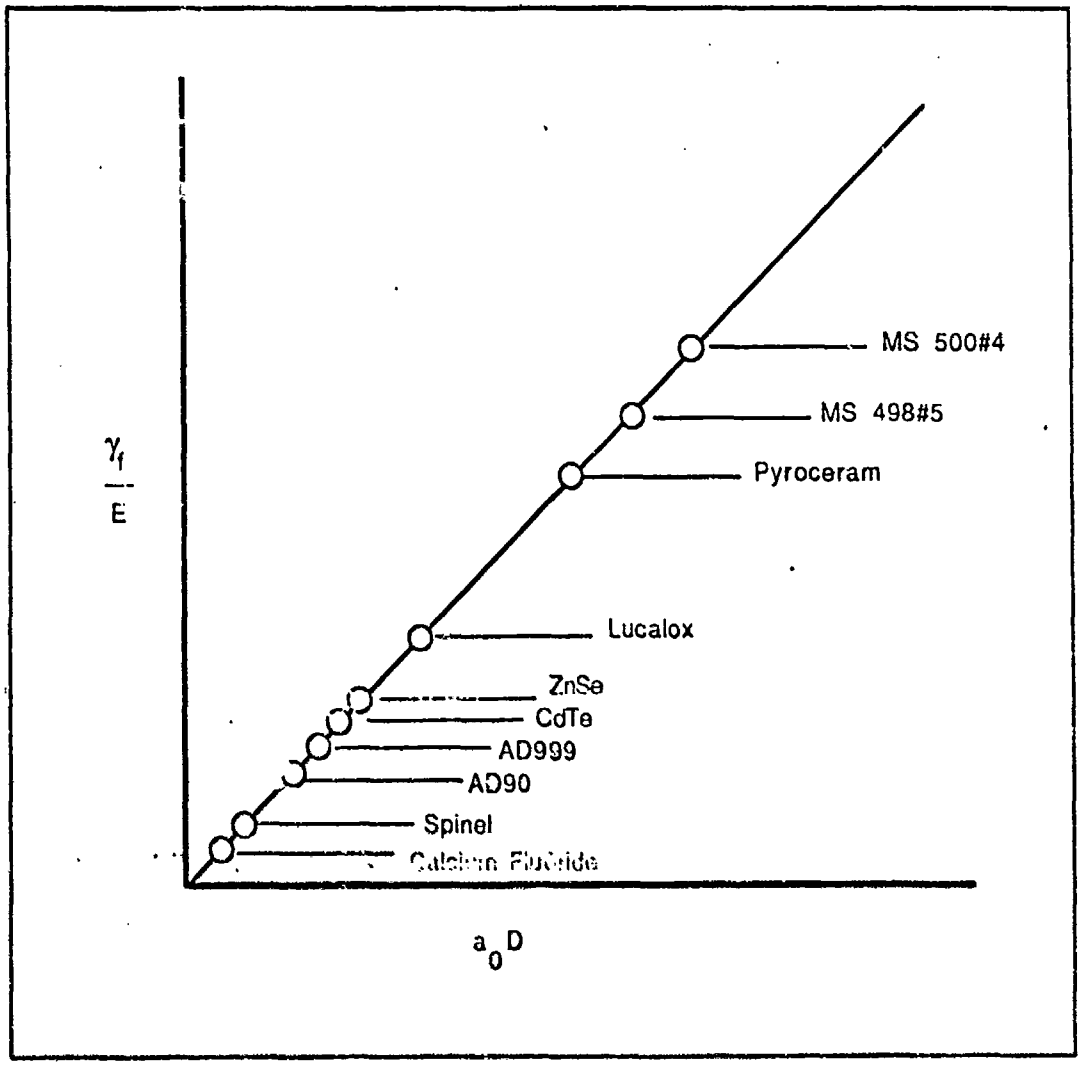

Figure 26. Plot of γ_f/E vs $a_0 D^*$.

More importantly, the vertical axis represents energy, the horizontal axis represents geometry. This implies an intimate connection between energy and geometry. Equation (28) provides a clear statement of this connection. Using fractal geometry, we may be better able to compute the actual fracture energies from fractal theoretic models.

Table III documents the calculated values for the characteristic length, a_0, for a number of materials. Notice that the single crystals and large grain polycrystals (ZnSe, CdTe) have characteristic lengths of a few angstroms. These values are of the order of lattice parameters and suggest that the unit process of fracture for these materials is on the order of atomic bond breaking. The zinc silicate glass ceramics show much larger characteristic lengths. This suggests that fracture of these materials is a cluster-like or molecular process.

TABLE III

Summary of the Calculated Values of Characteristic Length a_0

MATERIAL	γ(J/M^2)	E (GPa)	D	a_0 (Å)
Alumina				
AD90	11	390	1.21	3
AD999	19	406	1.31	3
Lucalox	26	305	1.31	5
Zinc Silicates				
MS 498#5	27	90	1.07	76
MS 500#4	27	89	1.12	53
Pyroceram	25	120	1.17	20
CdTe	1	40	1.20	3
ZnSe	5.5	69	1.30	4
CaF_2(s.c.)*	0.5	114	1.07	1
Spinel(s.c.)	3	240	1.09	3

* s.c. refers to single crystal

The determination of this characteristic length, a_0, is of startling significance. This length came about from a number of important assumptions. First, it is assumed that fracture is a fractal process. Further, it is assumed that this fractal process is scale invariant and self-similar. From this assumption, we propose that fracture on the macroscopic scale is composed of the scaled insertion of a unit process on the atomic scale. In other words, there is some small scale event with a definite geometric shape. This shape is repeated everywhere along the fracture and reveals its signature from the atomic to the macroscopic scales. Therefore, measurements of the geometric shape of fracture on the macroscopic scale can be used to infer the unit process on the atomic scale. Likewise, if we know the unit process, we can generate a shape. If we have a fractal dimension of a fracture surface, and we know something about the structure of the material, then we can deduce possible shapes for the unit process. We could then build a fracture surface from these shapes.

Our second assumption involves the family lines in K_{Ic} - D^* space. These lines have proposed slopes of 1/2. The slope of 1/2 was obtained from observations by Mecholsky et al. [24]

This assumes that all of the materials originally tested should lie along the same line (i.e., are members of the same family). It is not clear, however, that the zinc silicates should be in the same family with alumina.

The members of a particular family should exhibit similar fracture behavior. Their differences in toughness should reflect differences in crack geometry, not fundamental differences in fracture mechanisms. For example, consider a hypothetical material which is toughened by the addition of a second phase. This material would have three basic possibilities for crack propagation, only one of which would surely place it in the same family as the untoughened material:

(1) Fracture could pass through the second phase addition.

(2) Fracture could pass through the interface of matrix and second phase.

(3) Fracture could deflect around the second phase and remain entirely within the matrix.

Only the third possibility would represent a purely geometric toughening. The crack still "sees" the same material yet, because of deflection around the second phase, is forced to follow a longer path.

A series of heat treated Ocala cherts were obtained from Ed Beauchamp of Sandia National Labs. Purdy and Beauchamp[25] calculated a decrease in toughness as a result of heat treatment. Along with a decrease in toughness, there is a decrease in the qualitative fracture surface roughness.

In untreated chert, fracture propagates around zones of high density. Heat treatment improves the bonding at the zone boundaries and the crack now follows a less tortuous path through the dense zones. It may seem paradoxical that improved bonding results in a decrease in fracture toughness; yet the improved bonding allows the crack to propagate more smoothly, thereby generating less surface area.

The dominance of geometrical factors in affecting the toughness of Ocala chert suggested that these samples would constitute a family in the K_{Ic}-D^* plane. Figure 27 shows this data plotted in the toughness-fractal dimension plane. A least squares fit gives a slope that is, again, 0.5 . Figure 28 shows coastline sections for two of the Ocala chert samples; U5 and #4. Note the difference in roughness of these coastlines, and how this difference is quantified by the fractal dimension.

Another assumption that went into the determination of the characteristic length is the constant, **A**, of equation 23. The components of **A**, namely Young's modulus and the characteristic length, were derived from a dimensional analysis. We assured the existence of this length parameter by assuming that it was reasonable for Young's modulus to appear in equation (21). This is hinged upon the understanding that, ultimately, for a material to fracture, bonds must break. The elastic modulus provides an average measure of the strength of these bonds and, so, should appear in a model of fracture.

TABLE IV

Data Summary for the Ocala Cherts

Sample	Toughness	Fractal Dimension
U5	1.55	1.32
#3	1.46	1.26
#4	1.25	1.24
F5	1.05	1.17

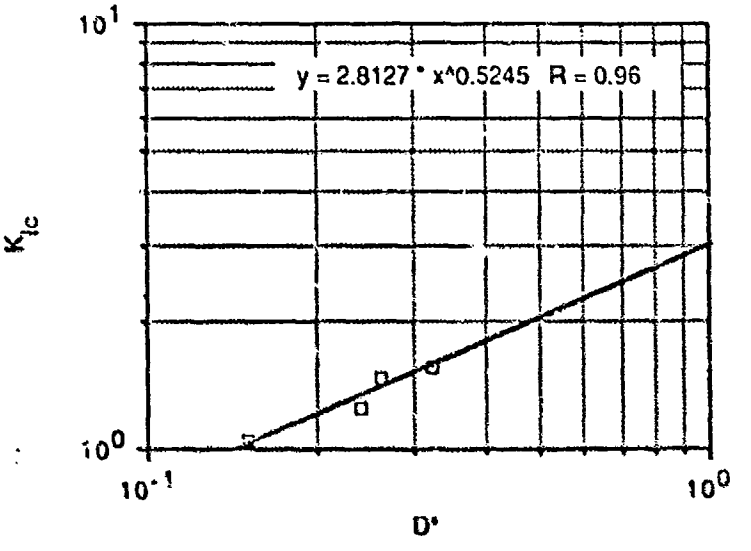

Figure 27. A plot of toughness against fractal dimension for the Ocala cherts again shows that: $K_{Ic} \sim D^{*1/2}$.

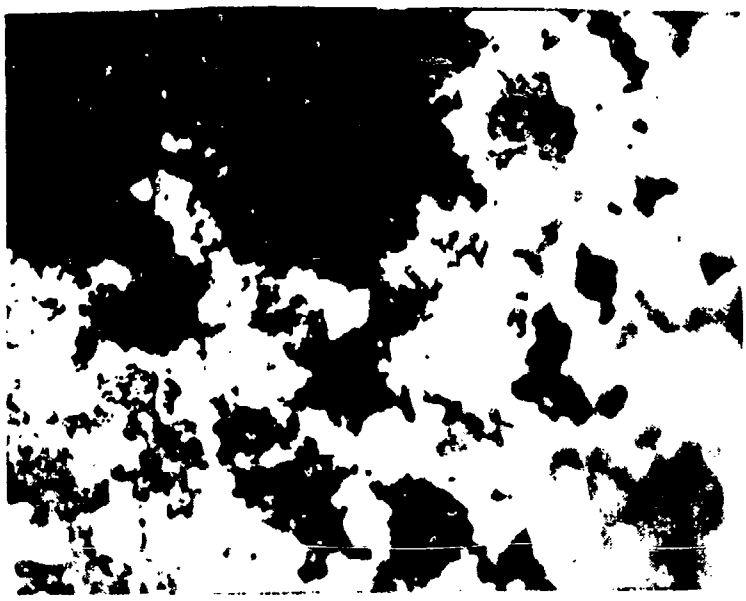

U5 chert, D = 1.32

#4 chert, D = 1.24

Figure 28. Sample coastlines for U5 and #4 chert samples.

Data Summary

Two techniques were used to determine the fractal dimension: Slit-island analysis and Richardson plots. Slit-island analysis uses area-perimeter data in the following equation:

$$A \sim P^{2/D}.$$

Therefore, $\log A \sim 2/D \log P.$

The slope of a graph of such data is equal to 2/D, where A, P, and D are as defined earlier.

Richardson plots employ the scale dependence of measured length in:

$$L = kE^{1-D}.$$

Therefore, $\log L = (1-D) \log E.$

The slope of such a relationship is equal to (1-D), where L ,E, and D are as defined earlier.

Figures 29 through 41 contain the data obtained from either Richardson or slit-island analysis for the materials listed in Table II. (This excludes the data of Mecholsky, Feinberg and Passoja.)

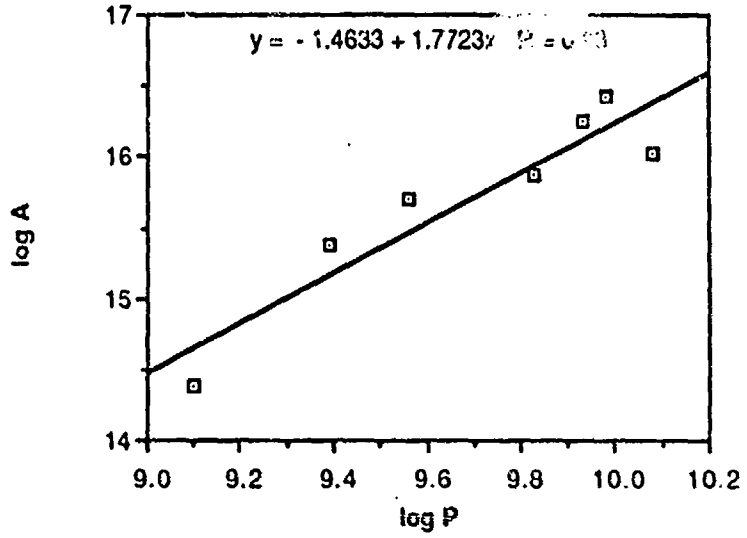

Slit-island plot
slope = 2/D
D = 1.13

Log A	Log P
14.39	9.10
15.38	9.39
15.70	9.56
15.87	9.83
16.03	10.08
16.25	9.93
16.42	9.98

Figure 29. Data for single crystal calcium fluoride

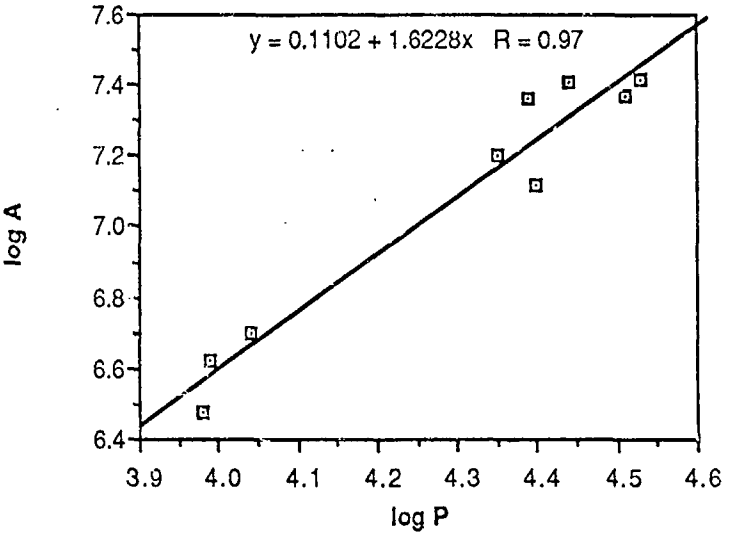

Slit-island plot
slope = 2/D
D = 1.23

Log A	Log P
6.48	3.98
6.62	3.99
6.70	4.04
7.12	4.40
7.20	4.35
7.37	4.51
7.36	4.39
7.42	4.53
7.41	4.44

Figure 30. Data for cadmium telluride

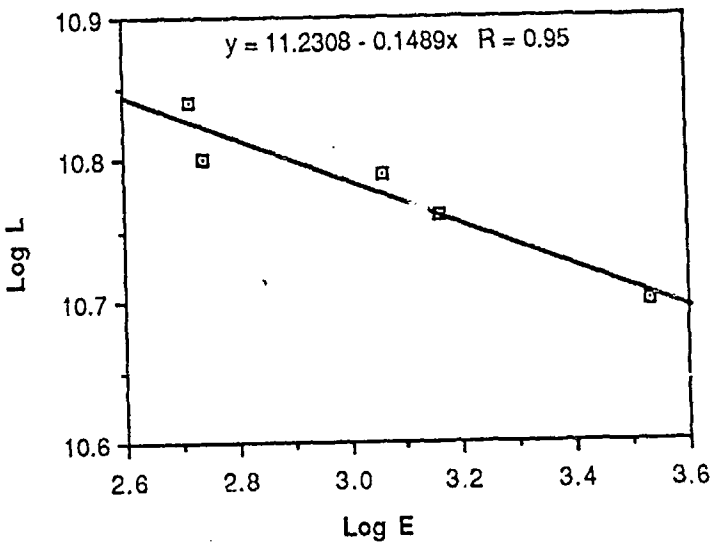

Richardson plot
slope = 1-D
D = 1.15

Log E	Log P
2.72	10.84
2.74	10.80
3.06	10.79
3.16	10.76
3.53	10.70

Figure 31. Data for F5 chert

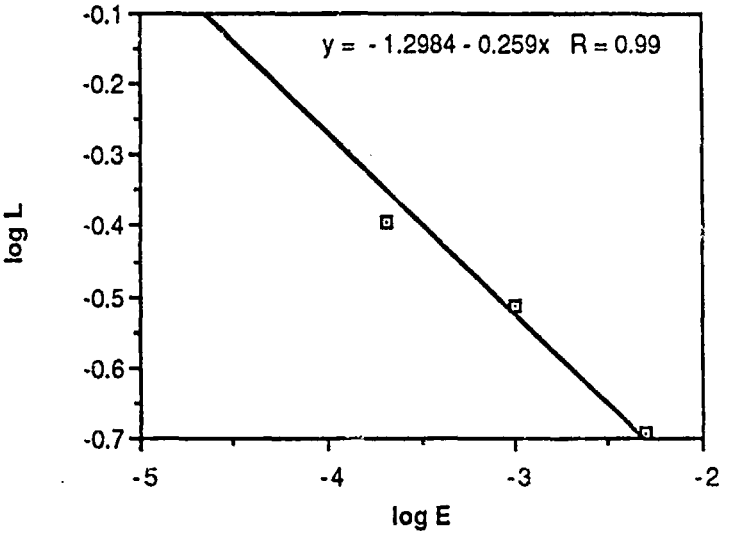

Richardson plot
slope = 1-D
D = 1.26

Log E	Log L
-2.30	-.693
-3.00	-.511
-3.69	-.393
-4.38	-.134

Figure 32. Data for chert #3

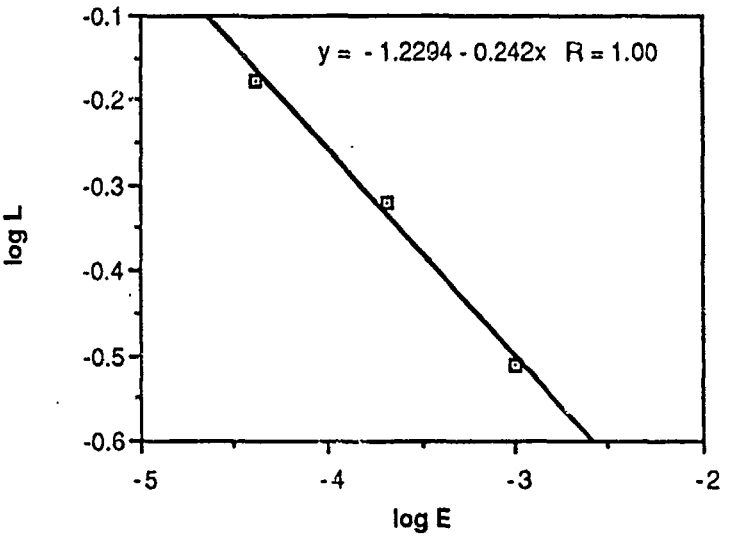

Richardson plot
slope = 1-D
D = 1.24

Log E	log L
-3	-.511
-3.69	-.321
-4.38	-.177

Figure 33. Data for chert #4.

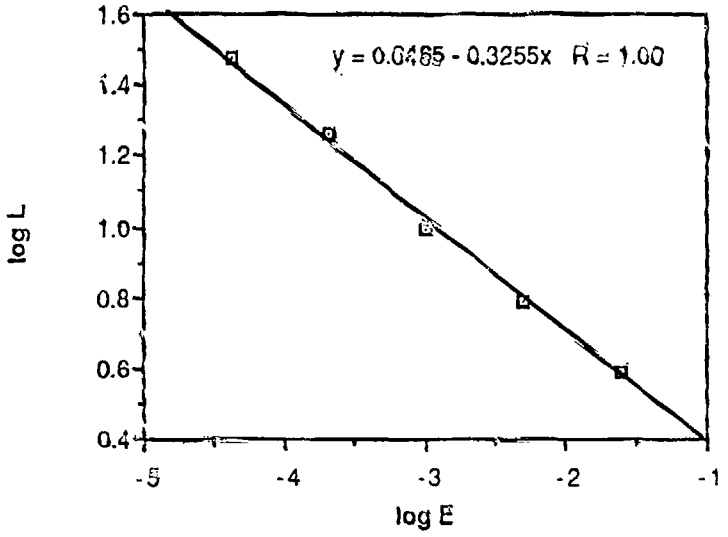

Richardson plot
slope = 1-D
D = 1.32

Log E	Log L
-1.61	.588
-2.30	.788
-3.00	.993
-3.69	1.26
-4.38	1.48

Figure 34. Data for U5 chert.

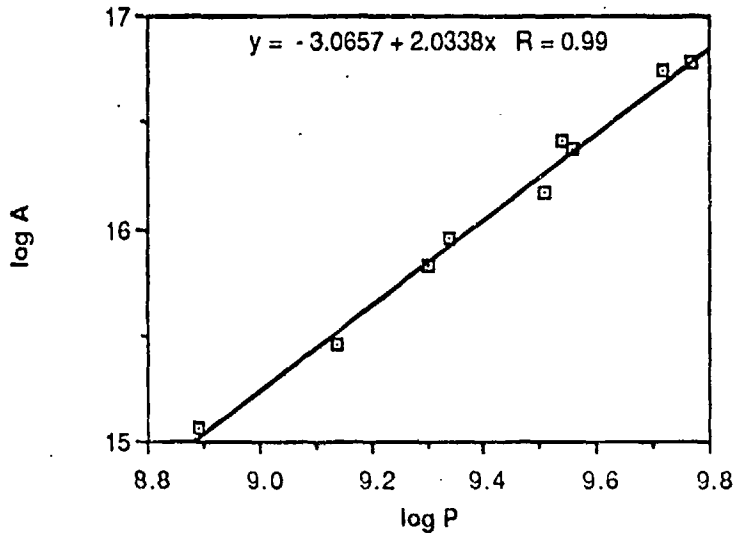

Slit-island plot
slope = 2/D
D = .98

Log A	Log P
15.06	8.89
15.46	9.14
15.63	9.30
15.96	9.34
16.17	9.51
16.38	9.56
16.42	9.54
16.78	9.77
16.75	9.72

Figure 35. Data for the Euclidean test sample.

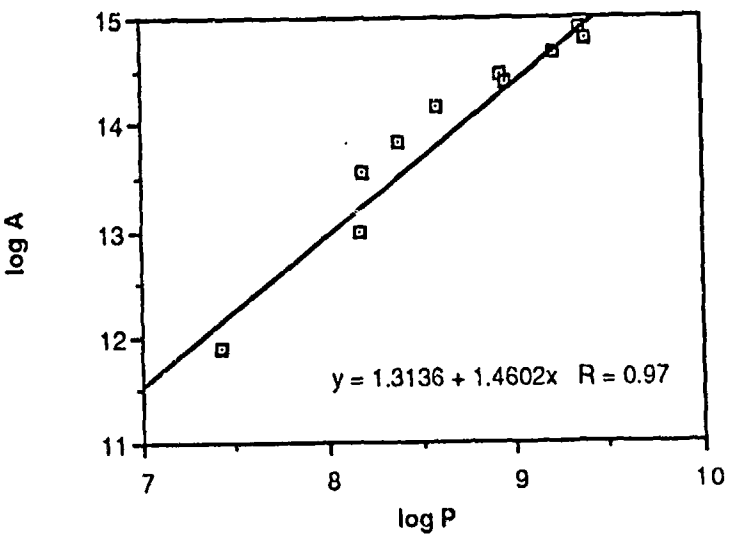

Slit-island plot
slope = 2/D
D = 1.37

Log A	Log P
11.90	7.43
12.99	8.18
13.54	8.19
13.82	8.39
14.15	8.59
14.39	8.96
14.47	8.93
14.66	9.22
14.80	9.38
14.91	9.36

Figure 36. Data for zinc silicate MS-508

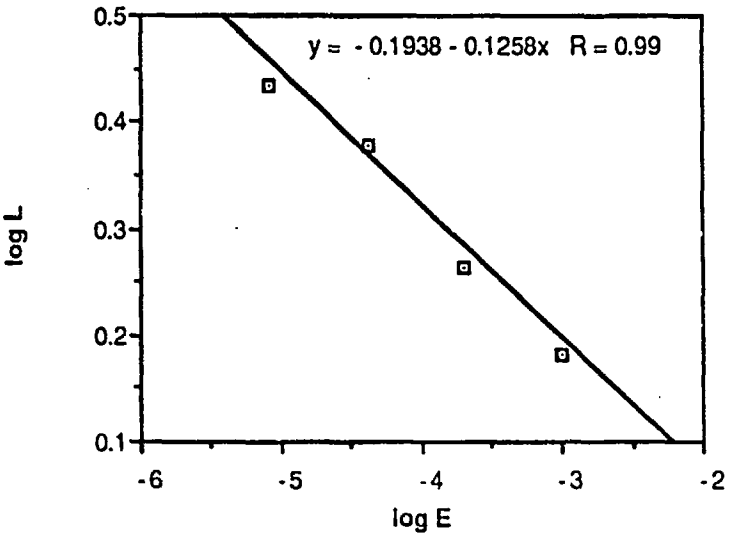

Richardson plot
slope = 1-D
D = 1.12

Log E	Log L
-3.00	.182
-3.69	.262
-4.38	.378
-5.08	.434

Figure 37. Data for polycrystalline spinel.

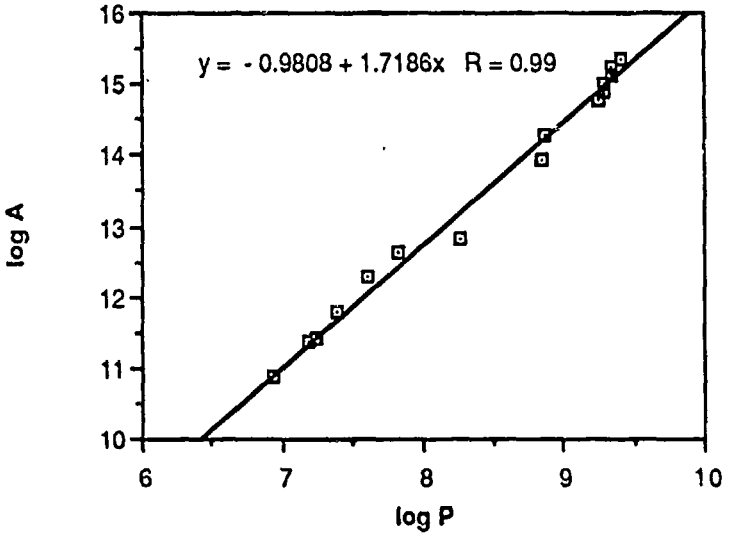

Slit-island plot
slope = 2/D
D = 1.16

Log A	Log P
12.62	7.82
12.82	8.26
11.80	7.38
13.95	8.85
14.29	8.87
12.31	7.61
14.77	9.25
14.91	9.29
15.01	9.29
15.12	9.34
10.88	6.94
15.22	9.35
11.39	7.18
15.34	9.42
11.42	7.25
15.36	9.42

Figure 38. Data for pyroceram.

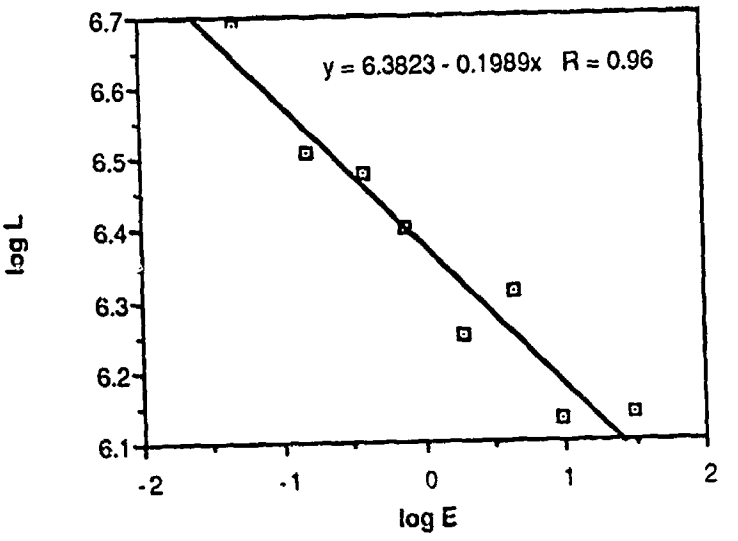

Richardson plot
slope = 1-D
D = 1.20

Log E	Log L
1.49	6.14
.982	6.13
.642	6.31
-.116	6.40
.285	6.25
-.405	6.48
-.812	6.51
-1.32	6.69

Figure 39. Data for PZT.

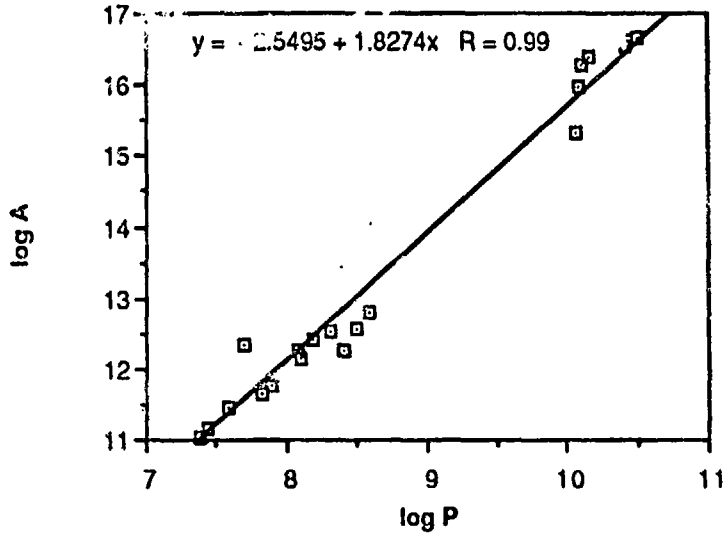

Slit-island plot
slope = 2/D
D = 1.09

Log A	Log P
15.32	10.06
12.33	7.70
15.98	10.08
16.26	10.10
16.37	10.16
16.55	10.42
11.65	7.82
11.16	7.43
11.76	7.89
11.02	7.39
16.61	10.44
12.15	8.10
11.47	7.58
16.67	10.51
12.27	8.08
12.28	8.40
12.43	8.19
12.55	8.49
12.53	8.32
12.79	8.58

Figure 40. Data for single crystal spinel

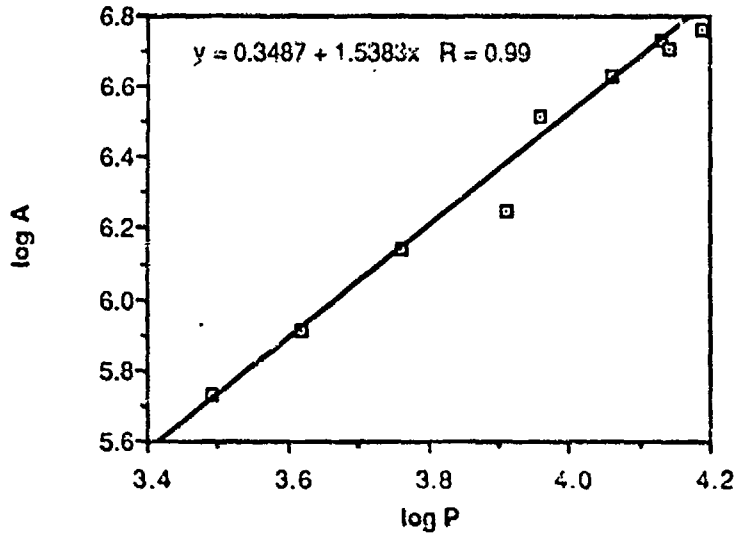

Slit-island plot
slope = 2/D
D = 1.30

Log A	Log P
5.73	3.49
5.91	3.62
6.14	3.76
6.25	3.91
6.52	3.96
6.63	4.06
6.71	4.14
6.73	4.13
6.76	4.19

Figure 41. Data for zinc selenide.

CHAPTER 4

CONCLUSIONS

The irregular structure of many fracture surfaces presents a picture that is too complicated for normal geometric description. A cross section through these surfaces will provide contour lines that are indicative of this complicated geometry. The length of these lines is related to the roughness and area of the surface from which it was derived. Therefore, classification of the dimension of such a line is useful in the description of the surface from which it was obtained. The basic constructs of fractal geometry give a simple methodology for categorizing the tortuosity of a line. Thus, fractals are used to classify the geometry of a line passing through a fracture surface.

A relationship is shown to exist between a material's fractal dimension and its fracture toughness;

$$K_{Ic} = A(D\text{-}1)^{1/2}.$$

The constant A is as a family parameter that groups materials in K_{Ic}-D^* space (where $D^* = D\text{-}1$). The value of this constant will identify a particular family line that may represent a fracture mechanism.

Assuming that fracture can be modeled as a scaling fractal, we proposed that the constant **A** is a product of Young's modulus and a characteristic length, a_0;

$$\mathbf{A} = E(a_0)^{1/2}.$$

Thus, it was possible to compute values of the characteristic length. Modeling fracture as a scaling fractal makes it possible to infer the atomic and microscopic geometric structure from the macroscopic geometric structure.

Fractal geometric modeling of fracture shows a number of encouraging results:

(1) The dimension of a line through a fracture surface gives an indication of the surface roughness, i.e., as D increases the surface roughness increases.

(2) D was shown to be related to fracture toughness. Within a given family: as D increases, toughness increases.

(3) Modeling the fracture surface as a scaling fractal permits the calculation of a characteristic length of fracture.

The use of scaling fractals allows for an orderly construction of a complicated geometric shape. Shapes that appear too chaotic for description find themselves well modeled by scaling fractals. Computer simulated landscapes, as found in Mandelbrot's book, are strikingly reminiscent of the natural world. It seems reasonable that these fractal models will be useful in describing the structure of the objects they simulate.

This thesis has shown that a fractal dimension can be assigned to brittle fracture surfaces. This dimension, as yet, is restricted to the description of contour lines on the fracture surface, as well as fracture surface profiles. It must be extended to the actual two-dimensional nature of the surface. The surface dimension will lie between two and three--two being a perfectly plane fracture. As the dimension increases from two to three, the surface will be increasing in roughness and geometric complexity. The relation between fractal dimension, fracture toughness, fracture surface roughness and surface area cannot be properly explored without the two-dimensional counterpart of the dimensions determined in this thesis.

It is clear that fracture models have taken no account of the tremendous complexity of fracture. In fact, the models assume that a crack simply separates planes of atoms into two perfectly plane fracture surfaces. The fractal approach will enable the accommodation of surface roughness into the basic models.

Instead of separating planes of atoms, the crack is allowed to wander. The new profiles generated by such a crack will be composed of shapes that resemble fractal generators. Thus, fracture surfaces can be constructed from atomic scale shapes that cascade, via the scale invariance of fractal geometry, to macroscopic fracture surface features. Computer simulations of this hypothesis are the next step in understanding the applicability of fractal concepts to brittle fracture.

REFERENCES

1. B. B. Mandelbrot, The Fractal Geometry of Nature, New York, W. H. Freeman (1982).

2. Ya. B. Zel'dovich and D. D. Sokolov, "Fractals, Similarity, Intermediate Asymptotics," Sov. Phys. Usp. 28(7), July (1985)

3. B. B. Mandelbrot, D. E. Passoja and A. J. Paullay, Nature, Vol. 308, 19 (1984)721.

4. S. Armentrout, Class notes "Fractals," Spring semester 1987, The Pennsylvania State University, Dept. of Mathematics.

5. K. Ravi-Chandar and W. G. Knauss, "An Experimental Investigation Into Dynamic Fracture: II Microstructural Aspects," Inter. J. of Fracture, 26 (1984) 65-80.

6. J. J. Mecholsky, S. W. Freiman and R. W. Rice, "Fracture Surface Analysis of Ceramics," J. Mater. Sci. (1976).

7. J. J. Mecholsky, S. W. Freiman and R. W. Rice, "Fractographic Analysis of Ceramics," ASTM STP 645, pp. 363-379 (1978).

8. E. B. Shand, "Breaking Stresses of Glass Determined from Dimensions of Fracture Mirrors," J. Am. Cer. Soc. 42(10) 474-477 (1959).

9. A. I. A. Abdel-Latif, R. C. Bradt and R. E. Tressler, "Multiple-Mist Regions on Glass Fracture Surfaces," in Fractography and Materials Science, ASTM STP 733,L.N. Gilbertson and R.D. Zipp, pp. 259-27 (1981).

10. J. W. Johnson and D. G. Holloway, "Microstructure of the Mist Zone on Glass Fracture Surfaces," Phil. Mag., 17, pp.899-910 (1968).

11. R. W. Davidge, Mechanical Behaviour of Ceramics, Cambridge; New York, Cambridge Univ. Press, (1979).

12. A. A. Griffith, "Phenomenon of Rupture and Flow in Solids," Phil. Trans. Royal Soc.(London), 221A(4) 163-98 (1920).

13. D. E. Passoja, "Fundamental Relationships Between Energy and Geometry in Fracture", Proc. of Conf. on Fractography, Alfred State Univ., Aug 1987 (to be published).

14. K. T. Faber and A. G. Evans, "Crack Deflection Processes - I. Theory," Acta Metall. Vol 31, No.4, pp.565-76, (1983).

15. Orowan, "Fracture and Strength of Solids," Rept. Progr. Phys, 12, 185-232 (1948).

16. J. J. Gilman, "Direct Measurements of the Surface Energies of Crystals," Journal of Applied Physics, Vol.31, No.12, pp.2208-18 (1960).

17. R. Koch, Dept. of Mathematics, Univ. of Oregon, Macintosh Public Domain Software Package, Fractal.

18. J. J. Mecholsky, T. J. Mackin and D. E. Passoja, "Self-Similar Crack Propagation in Brittle Materials," Proceedings of Conference on Fractography, Alfred State Univ. , Aug 1987 (to be published).

19. K. C. Feinberg, "Establishment of Fractal Dimensions for Brittle Fracture Surfaces," Senior Thesis, The Pennsylvania State University, (1985).

20. J. J. Mecholsky, T. J. Mackin and D. E. Passoja, "Crack Propagation in Brittle Materials as a Fractal Process," in Extended Abstracts, Fractal Aspects of Material, Materials Research Society, Dec. (1986).

21 J. J. Mecholsky and D. E. Passoja, "Fractals and Britlle Fracture," in Extended Abstracts, Fractal Aspects of Material , edited by R. B. Laibowitz, B. B. Mandelbrot and D. E. Passoja, Materials Research Society, Pittsburgh, PA. (1985).

22. B. B. Mandelbrot, D. E. Passoja and A. J. Paullay, "Fractal Character of Fracture Surfaces of Metals," Extended Abstracts in Fractal Aspects of Materials: Metal and Catalyst Surfaces, Powders and Aggregates, eds. B. B. Mandelbrot and D. E. Passoja, MRS, Pittsburgh, PA. pp.7-9 (1984).

23. D. E. Passoja and D. J. Amborski, "Fracture Profile Analysis by Fourier Transform Methods," Microstructural Science, 6, pp. 143-48 (1978).

24. J. J. Mecholsky, D. E. Passoja and K. C. Feinberg, "Quantitative Analysis of Brittle Fracture Surfaces Using Fractal Geometry," Submitted to J. Am. Cer. Soc. (1986).

25. E. K. Beauchamp and B. A. Purdy, "Decrease in Fracture Toughness of Chert by Heat Treatment,"(to be published).